© 2015. Published by The Company of Biologists Ltd | Development (2015) 142, 4385-4393 doi:10.1242/dev.129981

TECHNIQUES AND RESOURCES

RESEARCH ARTICLE

Expanding the power of recombinase-based labeling to uncover cellular diversity

Nicholas W. Plummer[1], Irina Y. Evsyukova[1], Sabrina D. Robertson[1,*], Jacqueline de Marchena[1], Charles J. Tucker[2] and Patricia Jensen[1,‡]

ABSTRACT

Investigating the developmental, structural and functional complexity of mammalian tissues and organs depends on identifying and gaining experimental access to diverse cell populations. Here, we describe a set of recombinase-responsive fluorescent indicator alleles in mice that significantly extends our ability to uncover cellular diversity by exploiting the intrinsic genetic signatures that uniquely define cell types. Using a recombinase-based intersectional strategy, these new alleles uniquely permit non-invasive labeling of cells defined by the overlap of up to three distinct gene expression domains. In response to different combinations of Cre, Flp and Dre recombinases, they express eGFP and/or tdTomato to allow the visualization of full cellular morphology. Here, we demonstrate the value of these features through a proof-of-principle analysis of the central noradrenergic system. We label previously inaccessible subpopulations of noradrenergic neurons to reveal details of their three-dimensional architecture and axon projection profiles. These new indicator alleles will provide experimental access to cell populations at unprecedented resolution, facilitating analysis of their developmental origin and anatomical, molecular and physiological properties.

KEY WORDS: Cre, Dre, Flp, Intersectional labeling, Norepinephrine

INTRODUCTION

Strategies and tools to label cells on the basis of gene expression provide the experimental framework for much of modern biology. By exploiting intrinsic genetic differences that uniquely define cell types, fluorescent labeling renders cells accessible for a wide variety of morphological, molecular, and physiological analyses. Although expression of fluorescent proteins can be controlled directly by cell-type-specific promoters, recombinase-based strategies (Dymecki and Tomasiewicz, 1998; Zinyk et al., 1998) constitute the key technology that gives gene-based labeling much of its power and flexibility. The use of a cell-type-specific recombinase driver allele in combination with an indicator allele encoding a fluorescent marker permits labeling on the basis of transient gene expression and, in the case of inducible recombinases, temporal control of labeling (reviewed in Jensen and Dymecki, 2014). Despite these refinements, however, labeling on the basis of a single gene defines relatively broad classes of cells (e.g. neurons synthesizing a specific neurotransmitter) and it is clear that this is only the tip of the cellular diversity iceberg.

In mice, access to more narrowly defined cell populations has been achieved using recombinase-based intersectional strategies, in which labeled cells occupy the narrow intersection of two broader gene expression domains (Awatramani et al., 2003). Intersectional labeling is accomplished with an indicator allele that is responsive to two distinct site-specific recombinases controlled by promoters of two different genes. Only those cells that have expressed both recombinases will express the marker encoded by the indicator allele. Additionally, some indicator alleles encode a second marker designed to label the subtractive population (Awatramani et al., 2003; Bang et al., 2012; Farago et al., 2006; Jensen et al., 2008; Yamamoto et al., 2009). The subtractive population consists of the balance of cells defined by one of the gene expression domains, minus the intersectional population (Farago et al., 2006). A labeled subtractive population provides important context for the intersectional population and, in some experiments, may actually be the population of interest. Intersectional and subtractive labeling can be applied to analysis of any tissue, but it has proved particularly useful in studies of the highly complex mammalian brain. This versatile approach has revealed previously unappreciated genetic and developmental heterogeneity within important neuronal classes (Awatramani et al., 2003; Bang et al., 2012; Cocas et al., 2009; Farago et al., 2006; Jensen et al., 2008; Miyoshi et al., 2010; Robertson et al., 2013; Sakamoto et al., 2014).

Despite the power of the intersectional approach, however, significant gaps remain in the toolkit. As development proceeds, genetically defined cell lineages become progressively subdivided by subsequent gene expression. It is becoming clear that a two-gene intersectional strategy, particularly when applied to the nervous system, provides insufficient resolution to dissect this complexity (Huang, 2014; Poulin et al., 2014). Furthermore, although some existing dual-recombinase-responsive indicator alleles have the capability of labeling cell bodies of the intersectional and subtractive populations (Awatramani et al., 2003; Bang et al., 2012; Farago et al., 2006; Jensen et al., 2008; Yamamoto et al., 2009), none are capable of labeling the axonal projections of the subtractive population. This restriction limits our ability to visualize the complete architecture of genetically defined neuronal populations.

Here, we describe a series of recombinase-responsive indicator alleles that overcome these deficiencies and significantly extend the utility of the intersectional approach. We have generated a new triple-recombinase-responsive fluorescent indicator allele that labels cell populations at the intersection of three independent gene expression domains. By taking advantage of the Dre-rox recombinase system (Sauer and McDermott, 2004), as well as the more commonly used Cre-loxP (Sternberg and Hamilton, 1981) and

[1]Neurobiology Laboratory, National Institute of Environmental Health Sciences, National Institutes of Health, Department of Health and Human Services, Research Triangle Park, NC 27709, USA. [2]Signal Transduction Laboratory, National Institute of Environmental Health Sciences, National Institutes of Health, Department of Health and Human Services, Research Triangle Park, NC 27709, USA.
*Present address: Biotechnology Program, Molecular Biomedical Sciences, North Carolina State University, Raleigh, NC 27695, USA.

‡Author for correspondence (patricia.jensen@nih.gov)

Received 24 August 2015; Accepted 9 November 2015

Development (2015) 142, 4385-4393 doi:10.1242/dev.129981

Flp-FRT (Andrews et al., 1985) systems, this allele offers unprecedented access to genetically defined cell types. A pair of dual-recombinase-responsive alleles allows labeling of Dre-Cre and Flp-Cre intersectional populations. Unlike any previously described indicator alleles, these three new alleles encode two fluorescent proteins that both fill cellular processes, allowing simultaneous tracing of axons of intersectional and subtractive populations. In addition, we have generated single-recombinase-responsive derivative alleles, including the first to provide a fluorescent readout of Dre expression.

We have observed expression of these alleles in adult mice and embryos, within and outside the nervous system. In conjunction with new tissue-clearing techniques, we have demonstrated the potential of our new indicator alleles by visualizing details of the heterogeneous architecture of the central noradrenergic system. The capability of these new alleles to label previously inaccessible intersectional and subtractive cell populations should prove valuable to a broad range of scientists, and their utility will only increase as more recombinase driver alleles are generated and characterized.

RESULTS

Generation of a new triple-recombinase-responsive fluorescent indicator and derivative alleles

To ensure expression of our new triple-recombinase-responsive fluorescent indicator allele, *RC::RFLTG* (Rosa-CAG-rox-FRT-loxP-tdTomato-eGFP), in a wide range of tissues and developmental stages, we used a synthetic CAG promoter (Niwa et al., 1991) and targeted the indicator construct to the *Gt(ROSA)26Sor* locus (Friedrich and Soriano, 1991) in mouse embryonic stem cells (Fig. 1A). *RC::RFLTG* expresses tdTomato after Dre-mediated deletion of a rox-flanked transcriptional stop cassette and Flp-mediated deletion of a FRT-flanked stop cassette. eGFP is expressed following Dre-, Flp- and Cre-mediated deletion of all stop cassettes and the loxP-flanked tdTomato. To generate dual- and single-recombinase-responsive alleles (Fig. 1A) and confirm that the stop cassettes can be efficiently recombined, we crossed *RC::RFLTG* mice with animals expressing Dre, Flp or Cre recombinase in the germline. Following recombinase expression in the predicted combinations, we observed ubiquitous fluorescence in intact mouse embryos (Fig. 1B) and a variety of intact organs in adult mice (Fig. S1), confirming that the indicator alleles are broadly expressed both pre- and postnatally. When one or more transcriptional stop cassettes remained intact, no fluorescence was observed in intact samples (Fig. 1B, Fig. S1).

To confirm the ability to detect expression of eGFP and tdTomato at the level of individual cells, we crossed our new alleles to recombinase driver lines with restricted expression patterns. In sections examined microscopically, we observed the expected eGFP and tdTomato fluorescence in a variety of neurons in embryos and adult brain (Fig. 2). In the absence of recombinase expression, we observed no tdTomato expression in brain and non-neuronal tissues. However, very faint eGFP fluorescence was occasionally observed in a few granule cells of the hippocampal dentate gyrus and scattered large cells of the choroid plexus. The absence of tdTomato expression suggests that the faint eGFP fluorescence does not result from 'leaky' transcription through the upstream stop cassettes. This low-level expression was virtually undetectable when tissue was labeled using anti-GFP antibody and fluorescently coupled secondary antibody (Fig. S2). Even under the most rigorous immunolabeling conditions using the most sensitive enzymatic detection method, it was fainter than in recombinase-expressing cells (Fig. S2). Therefore, it is not expected to limit the use of these new indicator alleles.

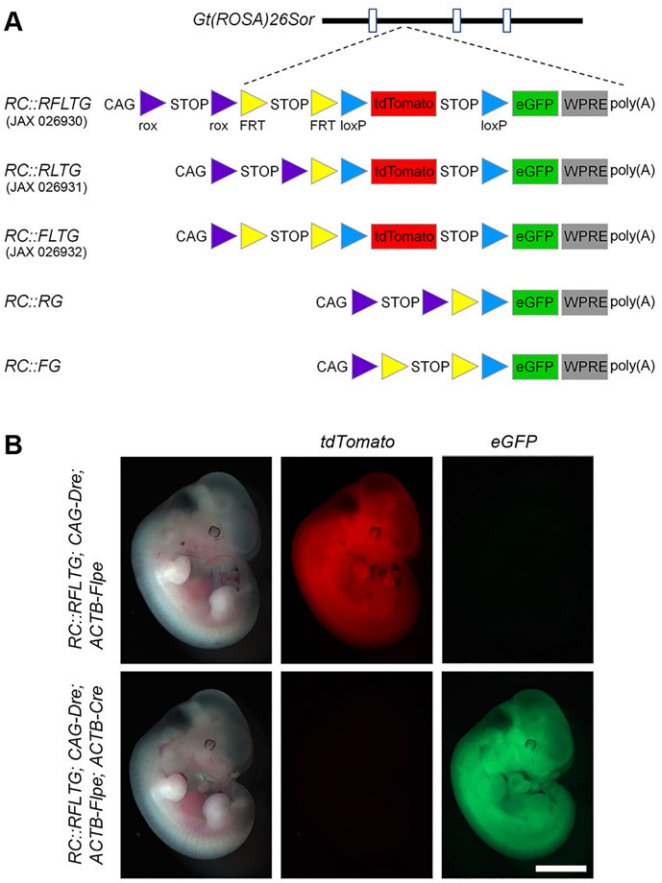

Fig. 1. A suite of recombinase-responsive fluorescent indicator alleles permits labeling of cells defined by expression of up to three different genes. (A) The triple-recombinase-responsive fluorescent indicator allele, *RC::RFLTG* (Rosa-CAG-rox-FRT-loxP-tdTomato-eGFP), was generated by targeting intron 1 of the *Gt(ROSA)26Sor* locus. Rox, FRT and loxP flanked transcriptional stop cassettes in *RC::RFLTG* (Jackson Lab, 026390) prevent expression of fluorescent protein in the absence of recombinase activity. The allele will express tdTomato in all cells with a history of Dre and Flp expression, and eGFP in all cells with a history of Dre, Flp and Cre expression. *RC::RLTG* (Jackson Lab, 026931) indicates history of Dre expression (tdTomato readout) and intersectional Dre-Cre expression (eGFP readout). *RC::FLTG* (Jackson Lab, 026932) indicates history of Flp expression (tdTomato readout) and intersectional Flp-Cre expression (eGFP readout). *RC::RG* and *RC::FG* indicate history of Dre or Flp expression, respectively (eGFP readout). CAG, synthetic CAG promoter (Niwa et al., 1991); STOP, His3-SV40 stop cassette (Sauer, 1993); WPRE, woodchuck hepatitis virus post-trascriptional regulatory element (Zufferery et al., 1999); poly(A), bovine growth hormone polyadenylation signal. (B) Expression of tdTomato but not eGFP is observed in E11.5 embryos after *RC::RFLTG* is recombined by ubiquitous Dre and Flp expression (*RC::RFLTG; CAG-Dre; ACTB-Flpe*; *n*=14). eGFP expression is observed after ubiquitous Dre, Flp and Cre expression (*RC::RFLTG; CAG-Dre; ACTB-Flpe; ACTB-Cre*; *n*=7). Images show native fluorescence. Scale bar: 2 mm.

To address recent reports of occasional Cre-mediated recombination of rox sites in transgenic mice and viral constructs (Fenno et al., 2014; Madisen et al., 2015), we performed a stringent test of this phenomenon. We crossed mice carrying our *RC::RG* allele, which contains a rox-flanked stop cassette (Fig. 1A), to *ACTB-Cre* (Lewandoski et al., 1997), which drives Cre expression in every cell of the mouse from the blastocyst stage or earlier. In double heterozygous offspring, we counted eGFP-labeled cells in every fourth section across the brain to determine the frequency of

Development (2015) 142, 4385-4393 doi:10.1242/dev.129981

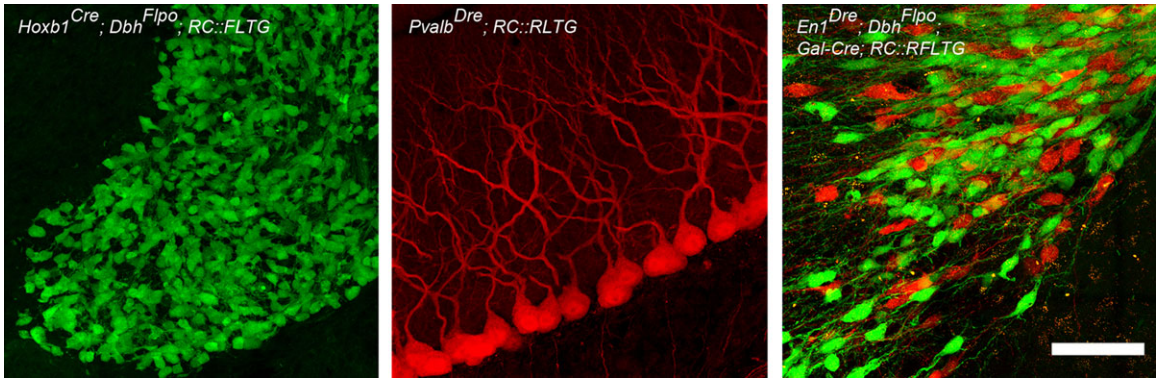

Fig. 2. Expression of eGFP and tdTomato from new indicator alleles permits visualization of individual cells. Various recombinase lines were used to drive expression of eGFP or tdTomato from *RC::FLTG*, *RC::RLTG* and *RC::RFLTG* in a variety of neuronal subtypes. Left, eGFP-labeled petrose ganglion in E14.5 embryo (*n*=2) heterozygous for *RC::FLTG*, *Hoxb1*^{Cre} (O'Gorman, 2005) and *Dbh*^{Flpo} (Robertson et al., 2013). Center, tdTomato-labeled purkinje neurons in mouse heterozygous for *RC::RLTG* and *Pvalb*^{Dre} (Madisen et al., 2015) (*n*=4). Right, eGFP- and tdTomato-labeled neurons in the locus coeruleus of mouse heterozygous for *RC::RFLTG*, *En1*^{Dre}, *Dbh*^{Flpo}, and *Gal-Cre* (Gong et al., 2007) (*n*=10). Images show native fluorescence. Scale bar: 83 µm (left), 53 µm (middle) or 100 µm (right).

Cre-mediated recombination of the rox-flanked stop cassette. We observed 2-7 labeled cells per mouse (*n*=4), indicating very low levels of Cre-rox recombination. Dre-mediated recombination of loxP sites has not previously been observed in transgenic mice (Madisen et al., 2015) but was reported in the context of highly expressed viral constructs (Fenno et al., 2014). To confirm that our alleles do not exhibit this cross-reactivity, we crossed the ubiquitously expressed *CAG-Dre* driver to a Cre-responsive eGFP indicator generated by germline deletion of the rox- and FRT-flanked stop cassettes from *RC::RFLTG*. No eGFP-labeled cells were observed (*n*=4 mice). Thus, the use of *RC::RFLTG* and *RC::RLTG* for intersectional analyses using Cre and Dre will not be limited by cross-reactivity of these two recombination systems.

Taken together, these results indicate that the promoter of *RC::RFLTG* and its derivatives remains broadly active throughout development, and the stop cassettes are capable of restricting expression of fluorescent protein. Therefore, these alleles are useful for labeling cells in any tissue of embryonic or adult mice for which appropriate recombinase driver lines are available, revealing their anatomical location and distinct morphology, and rendering them experimentally accessible.

New dual-recombinase-responsive indicator alleles offer significant advantages over previously described alleles

Several previously published Flp-Cre-responsive indicator alleles label cell bodies of intersectional and subtractive populations, but they are unable to label the axons of subtractive populations (Awatramani et al., 2003; Bang et al., 2012; Farago et al., 2006; Jensen et al., 2008; Yamamoto et al., 2009). The only previously published Dre-Cre-responsive indicator allele encodes a single fluorescent protein and is therefore incapable of labeling the subtractive population (Madisen et al., 2015). To determine whether our new alleles overcome these deficiencies, we applied our new Flp-Cre dual-recombinase-responsive allele, *RC::FLTG*, to analysis of the central noradrenergic system.

We recently used an intersectional genetic fate mapping strategy to determine the embryonic origins of central noradrenergic neurons (Robertson et al., 2013). Using a Flp-Cre indicator allele (Bang et al., 2012), a noradrenergic-specific Flp driver line (*Dbh*^{Flpo}) and available Cre driver lines, we identified four intersectional subpopulations of noradrenergic neurons that differ in their anatomical location and efferent projection pattern in the adult brain. However, a significant proportion of noradrenergic neurons were not included in any of the four intersectional populations. Therefore, their projections were not labeled by the indicator allele and we were unable to account for all noradrenergic inputs at target sites.

Here, we use our new Flp-Cre-responsive allele, *RC::FLTG*, in combination with *En1*^{Cre} (Kimmel et al., 2000) and *Dbh*^{Flpo}, to visualize projections from all noradrenergic neurons. The intersection of *En1* and *Dbh* expression domains (Fig. 3A) defines a subpopulation of noradrenergic neurons encompassing 99.8% of the functionally important locus coeruleus (LC) and a portion of the dorsal subcoeruleus (Robertson et al., 2013), according to an adult mouse brain atlas (Paxinos and Franklin, 2013). This intersectional subpopulation (hereafter designated the LC complex) is a major source of noradrenergic projections to the forebrain. The subtractive population consists of all remaining noradrenergic neurons.

In mice heterozygous for *En1*^{Cre}, *Dbh*^{Flpo} and *RC::FLTG*, we observed fluorescently labeled cell bodies and projections from both the intersectional (*En1*^{Cre}/*Dbh*^{Flpo}, eGFP-labeled) and subtractive (*Dbh*^{Flpo} expression only, tdTomato-labeled) noradrenergic populations (Fig. 3). Co-labeling with antibodies against tyrosine hydroxylase (TH) and norepinephrine transporter (NET) confirmed that *RC::FLTG* is efficiently recombined by these recombinase drivers (Fig. S3). The eGFP and tdTomato labeling allowed us to readily observe the distinct axonal morphologies of the two populations and their relative contribution to target regions within the same animal. In the brainstem, we were able to observe, for the first time, inputs to the locus coeruleus from all other noradrenergic neurons (Fig. 3B). In the forebrain, we could determine that axons originating in the LC complex are a minority of all noradrenergic inputs in the basolateral amygdala, bed nucleus of the stria terminalis (BNST) and paraventricular hypothalamus (Fig. 3C). The difference between the thin axons originating from the LC complex and the coarser axons with larger varicosities originating from other noradrenergic neurons (Robertson et al., 2013) was striking when the two populations were colabeled in the same tissue (Fig. 3C).

In regions where axons from the LC complex predominate, *RC::FLTG* allowed us to visualize inputs arising from all other noradrenergic populations. In the hippocampus, for instance, we observed a few tdTomato-labeled axons in every brain (*n*=5) that we examined (Fig. 3C, Fig. S3). This result contrasts with our previous

Development (2015) 142, 4385-4393 doi:10.1242/dev.129981

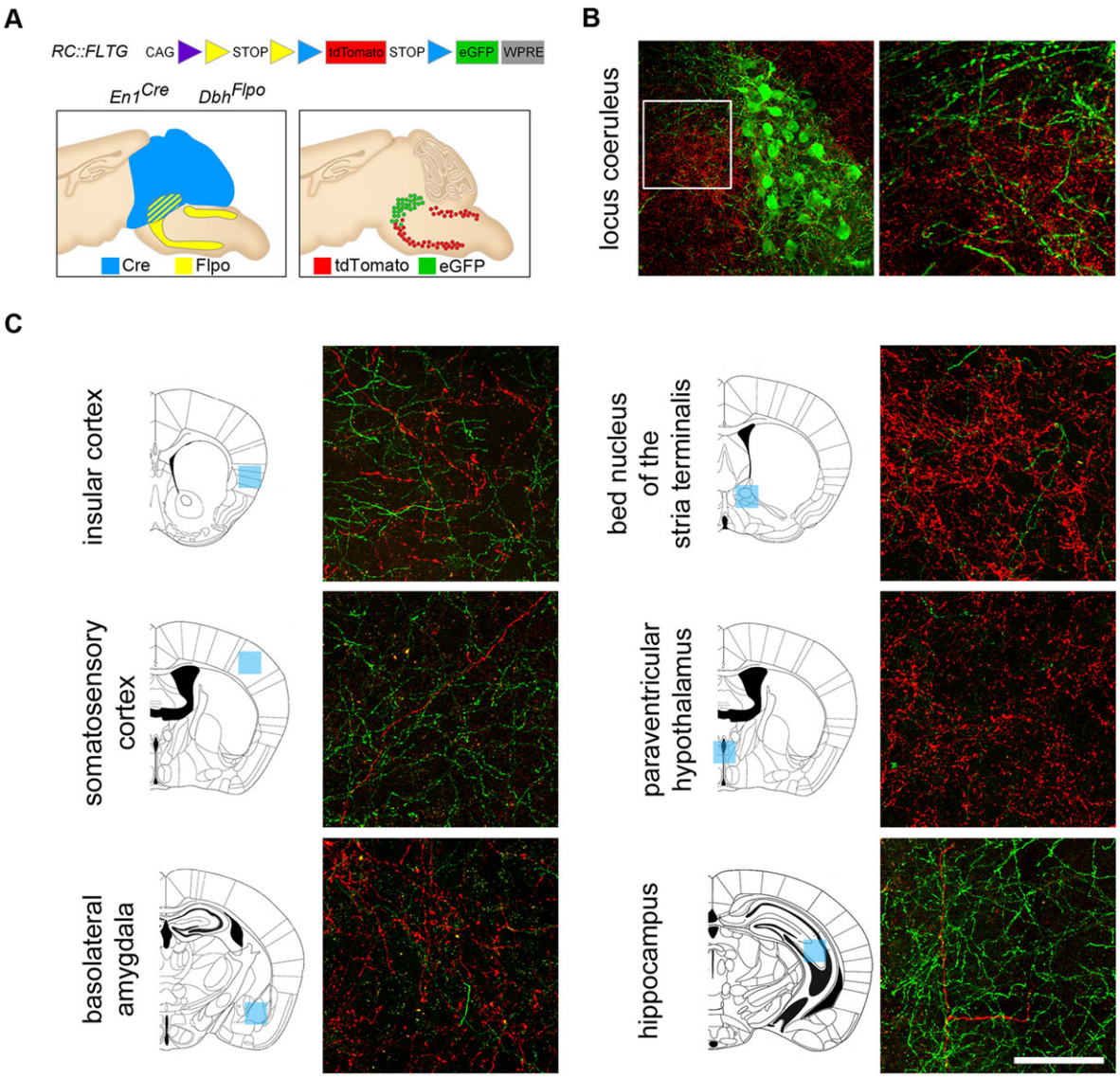

Fig. 3. Simultaneous labeling of axons from two genetically related neuronal subpopulations permits direct comparison of their projection profiles. (A) Intersectional labeling of two subpopulations of noradrenergic neurons in *En1*^{Cre}*; Dbh*^{Flpo}*; RC::FLTG* mice (*n*=5) is summarized in schematic sagittal views of the adult mouse brain. Cells with history of *En1*^{Cre} (blue) or *Dbh*^{Flpo} (yellow) expression occupy domains that overlap in the anterior hindbrain. Noradrenergic neurons with history of both *En1*^{Cre} and *Dbh*^{Flpo} expression are labeled with eGFP after deletion of the FRT-flanked transcriptional stop cassette and loxP-flanked tdTomato-stop in *RC::FLTG*. Noradrenergic neurons originating outside the *En1* domain express only *Dbh*^{Flpo}, resulting in deletion of the FRT-flanked stop cassette and labeling with tdTomato. Cells that do not express *Dbh*^{Flpo} are unlabeled because of the presence of the FRT-flanked stop cassette, regardless of Cre expression history. (B) The eGFP-labeled dendritic field of the locus coeruleus seen in coronal section (white box, enlarged on right) receives heavy input (tdTomato-labeled axons) from other populations of noradrenergic neurons. (C) At target sites of noradrenergic projections seen in coronal sections, the proportion of axons originating from the locus coeruleus complex relative to those originating from all other noradrenergic neurons can be observed. The projections from the LC complex are a minority of all noradrenergic axons in the bed nucleus of the stria terminalis (BNST; lateral division, ventral part), paraventricular hypothalamus and basolateral amygdala. In the hippocampus, rare but consistently observed tdTomato-labeled axons reveal, for the first time, noradrenergic inputs arising from neurons outside the LC complex. In the insular cortex, basolateral amygdala, BNST and paraventricular hypothalamus, the eGFP-labeled axons from the LC complex are finer with smaller varicosities compared with the tdTomato-labeled axons of other noradrenergic axons (Robertson et al., 2013). The blue boxes on the line diagrams show the approximate location of the imaged axons. Images show immunofluorescence. Scale bar: 50 µm (B, right and C) or 130 µm (B, left).

study, in which we observed only axons from the *En1*-derived LC complex in the hippocampus because of our inability to label projections from all noradrenergic neurons. This minor input to the hippocampus must originate from noradrenergic neurons located outside of the LC. The very small percentage (~0.2%) of LC neurons not derived from the *En1* expression domain is defined by early transient expression of *Hoxa2-Cre*, and that noradrenergic neuron population does not project to the hippocampus. Therefore, in *En1*^{Cre}*; Dbh*^{Flpo}*; RC::FLTG* brain, the tdTomato-labeled axons in the hippocampus arise from non-LC neurons not included in any of the four intersectional populations defined in our previous study (Robertson et al., 2013).

Taken together, these results confirm that the addition of a second fluorescent protein capable of filling cellular projections constitutes a significant improvement over existing dual-recombinase indicators. The ability to label, in isolation, a genetically defined

Development (2015) 142, 4385-4393 doi:10.1242/dev.129981

neuronal subpopulation and determine where it projects is a critical step in determining its function. Embedding an intersectional subpopulation in the context of a more broadly defined subtractive population permits comparisons, within a single animal, between different neuronal subtypes that previously would have required labor-intensive analysis of multiple intersectional crosses using several different Cre driver lines.

RC::RFLTG permits simultaneous intersectional labeling of cell bodies and axons from two neuronal subpopulations defined by overlapping expression of three genes

The intersectional strategy is a powerful method for gaining access to neuronal populations defined by complex combinatorial genetic signatures, but it is clear that subtype diversity exceeds the discriminatory power of dual-recombinase-responsive indicator alleles (Huang, 2014; Poulin et al., 2014). The characterization of additional recombinase systems such as Dre-rox now offers the possibility of capturing a larger proportion of the genetic heterogeneity in complex organs. To demonstrate the ability of our new triple-recombinase-responsive indicator, *RC::RFLTG*, to label cells defined by the intersection of three gene expression domains, we again turned to the central noradrenergic system.

As we have shown above, genetic access to the LC complex is achieved through a shared history of *En1* and *Dbh* expression. However, it is well established that neurons of the locus coeruleus are heterogeneous with respect to their axon projection profile, electrophysiological characteristics and expression of neuropeptides (Chandler and Waterhouse, 2012; Chandler et al., 2013, 2014; Holets et al., 1988; Olpe and Steinmann, 1991; Xu et al., 1998). Until now, it has not been possible to selectively label subpopulations of the LC complex. With its ability to label cells defined by the intersection of three gene expression domains, *RC::RFLTG* now provides access to these subpopulations and the capability to map their axonal projections to reveal potential functional differences.

To label two subpopulations of the LC complex based on neuropeptide expression, we used a Cre transgene driven by the promoter of the neuropeptide galanin (*Gal*) (Gong et al., 2007). This transgene is expressed in a subset of locus coeruleus neurons, but also elsewhere in the noradrenergic system and more widely in the brain (McCall et al., 2015; N.W.P. and P.J., unpublished observations). Our initial analysis of the *Gal-Cre*-expressing noradrenergic neurons in *Gal-Cre; Dbh^{Flpo}; RC::FLTG* mice demonstrated projections to brain regions that receive axons from the LC complex and from other noradrenergic populations. However, labeling of the entire noradrenergic system in these mice made it impossible to determine which projections arise from the LC complex (Fig. S4). Thus, a triple-recombinase approach was required to visualize projections from the *Gal-Cre*-expressing and *Gal-Cre*-negative subpopulations of the LC complex in isolation from all other cells.

To accomplish this goal, we bred mice heterozygous for *RC::RFLTG*, *Gal-Cre*, *Dbh^{Flpo}* (Robertson et al., 2013) and *$En1^{Dre}$* (N.W.P., J.d.M. and P.J., unpublished results). Although the expression patterns of these three recombinase drivers are very different, spatially and temporally, their intersection exclusively defines a subpopulation of noradrenergic neurons within the LC complex (Fig. 4). The subtractive population consists of the remaining neurons of the LC complex that do not express the *Gal-Cre* transgene, and all neurons outside the LC complex are unlabeled.

In hindbrains of *$En1^{Dre}$; Dbh^{Flpo}; Gal-Cre; RC::RFLTG* quadruple heterozygotes, we observed *Gal-Cre*-expressing (eGFP-labeled) and *Gal-Cre*-negative (tdTomato-labeled) noradrenergic neurons intermingled throughout the LC complex (Fig. 4). As with *RC::FLTG*, co-staining with TH and NET antibodies confirmed that *RC::RFLTG* is efficiently recombined by the recombinase drivers (Fig. S3). Next, we examined forebrain sections in order to observe the axonal projections from these two noradrenergic subpopulations and determine whether they project to distinct target sites. Labeled axons from both subpopulations were visible running together in the medial forebrain bundle. Surprisingly, we observed eGFP and tdTomato axons intermingled at all forebrain target sites (Fig. 4, Fig. S5). These results suggest that galanin may be required in all regions innervated by the LC complex.

These experiments demonstrate the unique ability of our triple-recombinase-responsive indicator allele to label in isolation subpopulations of cells that have never before been accessible. Compared with existing indicator alleles, *RC::RFLTG* can be used for deeper analysis of the complex gene expression patterns

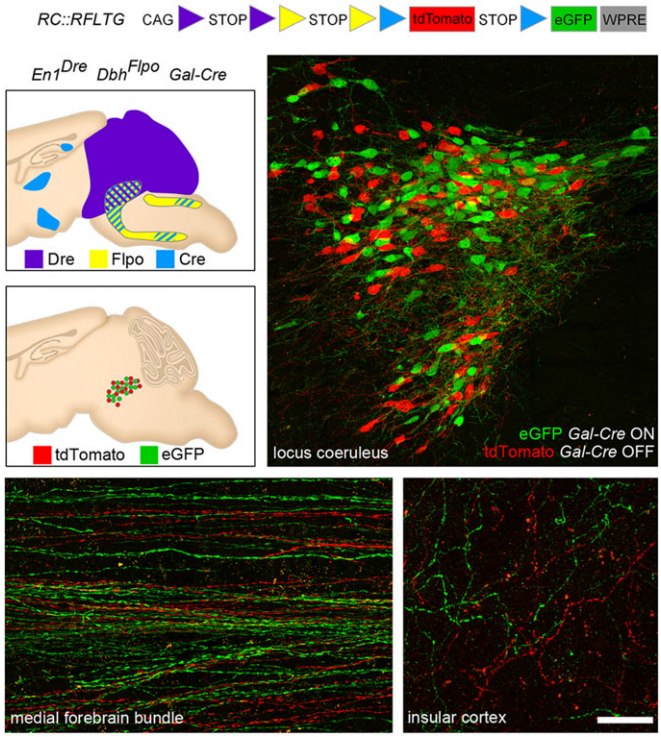

Fig. 4. Labeling cells defined by the expression of three genes increases cellular resolution, providing access to previously inaccessible cell populations. Schematic sagittal views of the adult mouse brain summarize expression of recombinases and fluorescent proteins in *$En1^{Dre}$; Dbh^{Flpo}; Gal-Cre; RC::RFLTG* quadruple heterozygotes (n=10). Neurons with history of *$En1^{Dre}$* (purple), *Dbh^{Flpo}* (yellow) or *Gal-Cre* (blue) expression occupy domains that overlap in the anterior hindbrain. eGFP expression is restricted to noradrenergic neurons with history of *$En1^{Dre}$*, *Dbh^{Flpo}* and *Gal-Cre* expression, which results in deletion of tdTomato and all transcriptional stop cassettes. tdTomato expression is restricted to neurons with a history of *$En1^{Dre}$* and *Dbh^{Flpo}* expression, without *Gal-Cre*, which results in deletion of the rox- and FRT-flanked stop cassettes. In sections, *Gal-Cre*-expressing (eGFP) and *Gal-Cre*-negative (tdTomato) noradrenergic neurons can be seen intermingled throughout the locus coeruleus. Labeled axons from both populations can be observed in the medial forebrain bundle and at cortical target sites. Locus coeruleus and medial forebrain bundle are shown in a sagittal section, rostral to left. The insular cortex is shown in a coronal section. Images show immunofluorescence. Scale bar: 100 µm (locus coeruleus), 38 µm (medial forebrain bundle), 22 µm (insular cortex).

Development (2015) 142, 4385-4393 doi:10.1242/dev.129981

underlying different cell types, and in combination with our new dual-recombinase-responsive alleles, it represents a significant expansion of the capabilities of the intersectional approach.

New indicator alleles are compatible with new tissue clearing techniques

Recently described techniques for rendering organs from mice and other animals optically transparent have made it practical to visualize the intact three-dimensional structure of fluorescently labeled cell populations, particularly neurons (Chung et al., 2013; Ertürk et al., 2012; Hama et al., 2011; Ke et al., 2013; Renier et al., 2014; Yang et al., 2014). Not only do these methods provide valuable information about the anatomical distribution and long-range connectivity of the labeled populations, but quantitative methods such as cell counting can be applied without labor-intensive and error-prone reconstruction from many different sections. To realize the full experimental utility of our new alleles, it is important that they are compatible with these techniques.

To test the compatibility of our alleles with the passive clarity technique (PACT) (Yang et al., 2014) and our ability to visualize complex neuronal populations in three dimensions, we cleared whole *Dbh*^{Flpo}*; RC::FLTG* embryos at E12.5 and 3-mm-thick slices of brain from adult *En1*^{Dre}*; Dbh*^{Flpo}*; Gal-Cre; RC::RFLTG* mice. In the embryos, we visualized the three-dimensional structure of the *Dbh*-expressing sympathetic ganglia. The intact, bilaterally symmetrical sympathetic chains were readily observed running on each side of the spinal column (Fig. S6). In the brain slices, the full morphology of the intact LC complex, including the *Gal-Cre*-expressing and *Gal-Cre*-negative subpopulations was visible (Fig. 5 and Movie 1). These neurons clearly form an unbroken continuum extending from the densely packed locus coeruleus to the more dispersed neurons in the dorsal subcoeruleus. Fluorescently labeled cells in 40-µm-thick virtual sections extending at least 500 µm deep in the tissue slice (Fig. 5) could be visualized as clearly as cells in 40-µm-thick free floating sections (Fig. 4). In cleared cerebral cortex, we were able to observe axons from both the *Gal-Cre*-expressing and *Gal-Cre*-negative subpopulations (Fig. 5). These results confirm that the combination of PACT and intersectional labeling using *RC::RFLTG* or its derivative alleles represents a powerful new method for visualizing the architecture of genetically defined cell types.

DISCUSSION

The experiments described here demonstrate that *RC::RFLTG* and its derivative alleles are a valuable toolkit of fluorescent indicators for noninvasive labeling of cell populations defined by one, two or three gene expression domains. Our proof-of-principle application of *RC::FLTG* and *RC::RFLTG* to analysis of the central noradrenergic system confirms the value of key features of these alleles. There are no molecular markers known to uniquely label subpopulations of noradrenergic neurons, so investigation of noradrenergic neuron heterogeneity, particularly axon projection patterns, depends either on genetic intersectional labeling (Robertson et al., 2013) or strategies for retrograde labeling by injection of dyes or viruses at target sites (Chandler and Waterhouse, 2012; Chandler et al., 2013, 2014; Schwarz et al., 2015). The ability of *RC::FLTG* to label axons of the entire noradrenergic system, subdivided between an intersectional and a subtractive population, reveals diversity of noradrenergic projections at target sites. As demonstrated in the hippocampus, our new allele allowed observation of previously undetected projections, without requiring the labeling of new intersectional populations. *RC::RLTG* offers the same features as *RC::FLTG* but adds to the flexibility of the intersectional approach by allowing dual-recombinase labeling with Dre and Cre.

As the first fluorescent indicator allele responsive to three recombinases, *RC::RFLTG* provides experimental access to previously inaccessible cell populations and thus is capable of detecting greater cellular diversity than any published indicator

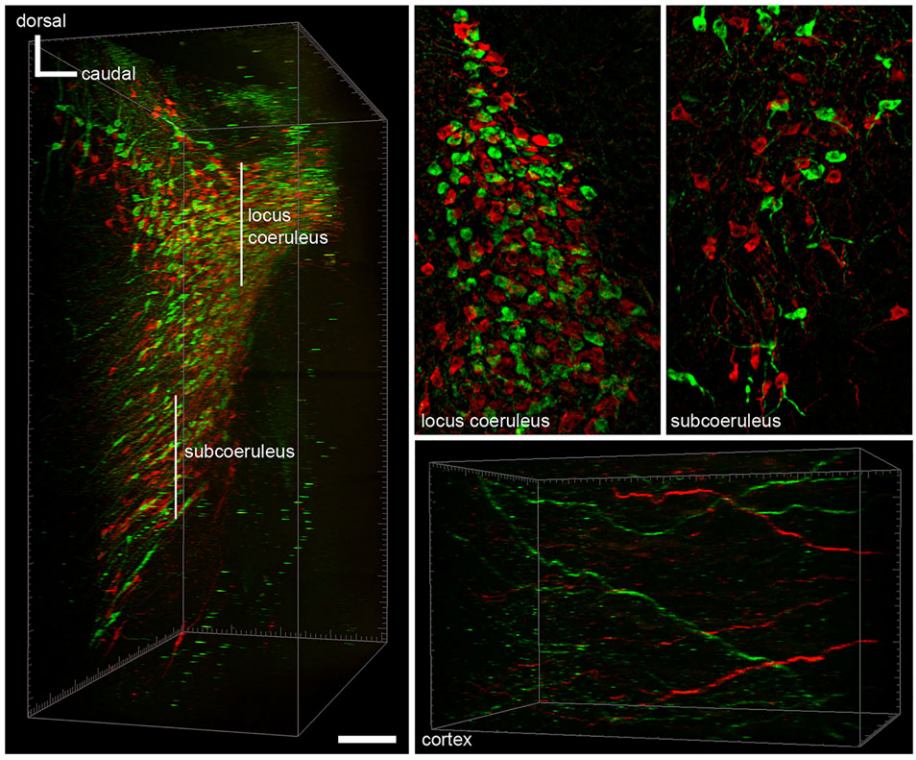

Fig. 5. Neurons and their axonal projections labeled by expression of eGFP and tdTomato from *RC::RFLTG* can be observed within intact brain tissue cleared by the passive clarity technique. Left: In cleared 3-mm-thick coronal slices of *En1*^{Dre}*; Dbh*^{Flpo}*; Gal-Cre; RC::RFLTG* quadruple heterozygous brain (*n*=3), the shape of the LC complex, including the spatial relationship between the dense locus coeruleus and more dispersed subcoeruleus regions, can be seen in a 3D reconstruction. Center: *Gal-Cre*-expressing (eGFP) and *Gal-Cre*-negative (tdTomato) neurons of the locus coeruleus are visible in a maximum intensity projection (MIP) compressed along the rostrocaudal axis of a 40-µm-thick region beginning 460 µm from the rostral surface of the tissue. Right: Neurons of the dorsal subcoeruleus are visible in a 40 µm MIP beginning 280 µm from the rostral surface. The two MIPs are viewed with the medial side of the subpopulation to the left, and their approximate locations are indicated by vertical lines on the 3D reconstruction. Bottom: In a 220 µm MIP from a 3 mm slice of forebrain viewed on the *z-y* plane, axons from both the *Gal-Cre*-expressing and *Gal-Cre*-negative subpopulations can be observed running in a rostrocaudal orientation within the cortex. Images show immunofluorescence. Scale bar: 200 µm (entire subpopulation), 86 µm (locus coeruleus and subcoeruleus), 30 µm (cortex).

Development (2015) 142, 4385-4393 doi:10.1242/dev.129981

allele. This unique capability allowed us, for the first time, to visualize two locus coeruleus subpopulations distinguished by *Gal-Cre* expression in isolation from all other cells. Wide-ranging evidence indicates the importance of galanin in noradrenergic neurons and possible functional differences between galanergic and non-galanergic LC neurons (Sevcik et al., 1993; Miller et al., 1999; Sciolino et al., 2015). However, despite evidence that the LC contains neurons with distinct projection profiles (Chandler and Waterhouse, 2012; Chandler et al., 2013, 2014), the subpopulations distinguished by *Gal-Cre* expression show no gross difference in their axonal targets. This surprising result is compatible with the recently reported finding that specifically activating the *Gal-Cre*-expressing LC subpopulation has the same effect on aversive behavior as activating the whole LC (McCall et al., 2015).

In addition to revealing the anatomic distribution and axonal projection patterns of neuronal populations, *RC::RFLTG* and its derivative alleles will render labeled cells accessible for morphometric analyses, electrophysiological recording, gene expression profiling and sorting from acutely dissociated tissue. With the rapidly expanding use of Dre and Flp recombinases, our new Dre- and Flp-responsive alleles, *RC::RG* and *RC::FG*, are important additions to the genetic toolkit. These single-recombinase-responsive alleles label all cells that have a history of Dre or Flp expression with eGFP, permitting rapid characterization of the driver lines used in more-complex intersectional experiments. *RC::RLTG* and *RC::FLTG* also function as Dre or Flp single recombinase indicators, respectively, with readout of tdTomato. Therefore, our alleles permit flexibility in the choice of fluorophores for experiments combining the indicator alleles with other fluorescent molecules. *RC::RLTG* and *RC::RG* are the first indicator alleles to provide a fluorescent readout of Dre expression.

Increased use of intersectional strategies for labeling and functional manipulation of restricted cell populations (Duan et al., 2014; Fenno et al., 2014; Hermann et al., 2014; Kim et al., 2009; Madisen et al., 2015) will undoubtedly lead to development of an array of new Dre and Flp driver lines to rival the existing inventory of Cre lines. However, in the absence of mouse lines with the desired recombinase expression pattern, one or more of the recombinases can also be delivered virally, rendering *RC::RFLTG* and its derivatives broadly useful for further dissection of cell types that have been defined by dual- or single-recombinase strategies. Combining our new indicator alleles with stereotaxic injections of a recombinase-expressing viral vector will permit access to subsets of genetically defined cell populations that are distributed among more than one anatomical location. Alternatively, retrograde-transported viruses (Kato et al., 2011; Soudais et al., 2001) can be used in the nervous system to subdivide populations on the basis of axonal target sites.

In summary, we have generated, characterized and demonstrated the use of a new suite of mouse lines for labeling genetically defined cell populations at any stage of development. The expression of eGFP and tdTomato from these alleles is capable of revealing cell morphology, including the axonal projection profile, of two neuronal subpopulations simultaneously and they are compatible with tissue clearing techniques. While these features make our new alleles particularly useful in neuroscience research, they will also be important tools for dissection of developmental and genetic complexity in a wide range of biological systems.

MATERIALS AND METHODS

Generation of new mouse strains

The pRC-RFLTG targeting vector was generated by insertion of a CAG promoter, rox-flanked His3-SV40 stop cassette, FRT-flanked His3-SV40 stop cassette, loxP-flanked tdTomato-stop and eGFP cDNA into the *Gt(ROSA)26Sor* targeting vector pAi9 (Madisen et al., 2010) after digestion with *Pac*I and *Fse*I (see supplementary Materials and Methods). Linearized pRC-RFLTG was electroporated into G4 embryonic stem cells (George et al., 2007) obtained from the Lunenfeld-Tanenbaum Research Institute, Mt Sinai Hospital, Toronto, ON, Canada. Homologous recombinants were identified by long-range PCR using the Expand long range dNTP pack (Roche Diagnostics) and primers specific for the 5′ and 3′ ends of the recombinant locus. Southern blots probed for the neomycin resistance gene were used to confirm absence of random integrations. The karyotypes of recombinant clones were assessed, and several clones were transfected with pPGKPhiC31obpa (Raymond and Soriano, 2007) to remove the attB-attP-flanked Neo cassette. The clones were then injected into B6(Cg)-Tyr^{c-2J}/J blastocysts to produce chimeric mice and male chimeras were bred to female C57BL/6J mice to establish the *RC::RFLTG* mouse line.

The *RC::FLTG* derivative strain was established by breeding *RC::RFLTG* chimeras with B6;129-*Tg(CAG-dre)1Afst* mice (Anastassiadis et al., 2009) (*CAG-Dre*), which express Dre recombinase in the germline. *R/C::RLTG* was established by crossing *RC::RFLTG* with B6.Cg-*Tg(ACTFlpe)9205Dym/J* mice (Rodriguez et al., 2000) (*ACTB-Flpe*; Jackson Laboratory, 005703), which express Flp recombinase in the germline. *RC::RG* and *RC::FG* mice were generated by crossing B6;FVB-*Tg(ACTB-cre)2Mrt* mice (Lewandoski et al., 1997) (*ACTB-Cre*) with *RC:RLTG* and *RC::FLTG*, respectively. Each derivative strain was maintained by back-crossing to C57BL/6J mice. *RC::RFLTG* (stock no. 026930), *RC::RLTG* (stock no. 026931) and *RC::FLTG* (stock no. 026932) mice are available from the Jackson Laboratory.

Experimental crosses

To test expression of *RC::RFLTG* and its derivatives in various adult tissues and during embryonic development, we first deleted both the rox- and FRT-flanked stop cassettes by crossing *RC::RFLTG* with an animal hemizygous for both *CAG-Dre* and *ACTB-Flpe*. In offspring inheriting all three transgenes, tdTomato demonstrates expression of the recombined indicator allele. Mice carrying the recombinant allele were then crossed with *ACTB-Cre* hemizygotes by timed mating and embryos were collected at E11.5 to demonstrate expression of eGFP after Cre-mediated excision of the tdTomato cassette. Breeding $En1^{Dre}$; Dbh^{Flpo}; *Gal-Cre; RC::RFLTG* quadruple heterozygotes required several crosses. First, B6;129-$Dbh^{tm1(Flpo)Pjen}$ mice (Robertson et al., 2013) (Dbh^{Flpo}) were crossed with *RC::RFLTG* mice and offspring were back-crossed to generate animals heterozygous for Dbh^{Flpo} and homozygous for the indicator allele. Mice heterozygous for the $En1^{Dre}$ knock-in allele (N.W.P., J.d.M. and P.J., unpublished results) were crossed with STOCK *Tg(Gal-cre)K187Gsat* hemizygotes (Gong et al., 2007) (*Gal-Cre*; MMRRC, 031060-UCD) and offspring were back-crossed to $En1^{Dre}$ to generate animals hemizygous for *Gal-Cre* and homozygous for $En1^{Dre}$. Finally, Dbh^{Flpo}; *RC::RFLTG* mice were crossed with $En1^{Dre}$; *Gal-Cre* mice to generate the $En1^{Dre}$; Dbh^{Flpo}; *Gal-Cre; RC::RFLTG* quadruple heterozygotes and control genotypes. $En1^{Cre}$; Dbh^{Flpo}; *RC::FLTG* and $Hoxb1^{Cre}$; Dbh^{Flpo}; *RC::FLTG* triple heterozygotes were generated by crossing B6.Cg-$En1^{tm2(cre)Wrst}$ heterozygotes (Kimmel et al., 2000) or B6;129-$Hoxb1^{tm1(cre)Og}$ heterozygotes (O'Gorman, 2005) (Jackson Laboratory, 012373) with mice heterozygous for Dbh^{Flpo} and homozygous for *RC::FLTG*. B6.Cg-$Pvalb^{tm3.1(dreo)Hze}$/J heterozygotes (Madisen et al., 2015) ($Pvalb^{Dre}$; Jackson Laboratory, 021190) were crossed with *RC::RLTG* to generate double heterozygotes.

All mice were maintained on a 12 h light:12 h dark cycle with food and water *ad libitum*, and either singly or group housed. Both male and female mice were examined. Unless otherwise indicated, all mice examined were adults aged 5 weeks or older. Sample sizes were not predetermined statistically but are similar to those reported previously (Bang et al., 2012; Robertson et al., 2013). Investigators did not collect data blind to genotype, because the fluorescent labeling in each cross and genotype is so distinctive that they would be easily recognized. All mouse experiments were performed with approval of the National Institute of Environmental Health Sciences (NIEHS) Institutional Animal Care and Use Committee.

Development (2015) 142, 4385-4393 doi:10.1242/dev.129981

Imaging of native fluorescence from new indicator alleles

For imaging native eGFP and tdTomato fluorescence, embryos were fixed overnight by immersion in 4% paraformaldehyde (PFA) in 0.01 M phosphate-buffered saline (PBS) at 4°C. Adult mice were anesthetized with sodium pentobarbital and transcardially perfused with PBS followed by 4% PFA in PBS. After dissection, the brains and other organs were postfixed overnight in 4% PFA at 4°C and rinsed in PBS before equilibration in 30% sucrose in PBS for 48 h at 4°C. Before sectioning on a Leica CM3050 S cryostat (Leica Biosystems), the cryoprotected samples were embedded in tissue freezing medium (General Data Company). Free-floating 40-µm-thick sections were mounted on microscope slides and coverslips were added using Vectashield (Vector Laboratories) before imaging.

Antibodies and immunohistochemistry

For immunohistochemistry, mice were perfused and sections collected as described above. Immunofluorescent labeling was performed on free-floating coronal or sagittal sections. Neurons expressing tdTomato were detected using rabbit anti-dsRed primary antibody (1:1000; Clontech Laboratories, 632496) and Alexa Fluor 568 goat anti-rabbit secondary antibody (1:1000; Life Technologies, A11036) and eGFP-expressing neurons were detected using chicken anti-GFP primary antibody (1:10,000; Abcam, ab13970) and Alexa Fluor 488 goat anti-chicken secondary antibody (1:1000; Life Technologies, A11039) (Robertson et al., 2013). For tissue cleared by the passive clarity technique (PACT; see supplementary Materials and Methods), the rabbit anti-dsRed (1:500) and chicken anti-GFP (1:1000) primary antibodies were detected using Alexa Fluor 568 donkey anti-rabbit F(ab′)2 fragments (1:500; Abcam, Ab175694) and Alexa Fluor 488 donkey anti-chicken F(ab′)2 fragments (1:500; Jackson Laboratory, 703-546-155). Noradrenergic identify of labeled axons was confimed using mouse monoclonal anti-NET (1:1000; clone NET-05; PhosphoSolutions, 1447-NET) (Matthies et al., 2009) and Alexa Fluor 633 goat anti-mouse secondary antibody (1:1000; Life Technologies, A21052). Noradrenergic identity of fluorescently labeled neuronal cell bodies was confirmed using mouse monoclonal anti-TH (1:500, clone 185; GeneTex, GTX10372) (Lundgren et al., 2011) and Alexa Fluor 633 goat anti-mouse secondary antibody. After staining, sections were mounted on microscope slides for imaging. For 4′,6-diamidino-2-phenylindole (DAPI) staining of nuclei, slide-mounted sections were incubated in 1 µg/ml DAPI in PBS for 1 min, followed by two 5 min washes in PBS prior to cover slipping.

For the highest sensitivity detection of faint eGFP expression in dentate gyrus and choroid plexus cells, we used immunoperoxidase labeling on 40-µm-thick free-floating sections. We used the chicken anti-GFP antibody (1:10,000) in conjunction with a biotinylated goat anti-chicken secondary antibody (1:500; Vector Laboratories, BA-9010). To detect immunoreactivity, we used the Vectastain Elite ABC kit and Vector SG substrate (both Vector Laboratories). To allow for maximal staining, the sections were incubated in the Vector SG solution for 15 min, the longest incubation time recommended by the manufacturer. For comparison of staining in noradrenergic neurons, dentate gyrus and choroid plexus, free-floating sections from the same brain were stained in the same experiment and then imaged using identical exposure settings.

Assessment of cross-reactivity between Cre-loxP and Dre-rox recombinase systems

To assess the frequency of Cre-mediated recombination of the rox-flanked stop cassette, we generated mice hemizygous for *ACTB-Cre* and heterozygous for *RC::RG*. In these mice, eGFP indicates recombination of rox sites by Cre. To assess Dre-mediated recombination of loxP sites, we crossed *RC::RFLTG* with *CAG-Dre* and *ACTB-Flpe* to excise the rox- and FRT-flanked stop cassettes. After backcrossing to C57BL6/J, the mice were again crossed to *CAG-Dre*. In these mice, eGFP indicates recombination of loxP sites by Dre. After perfusion, each brain was completely sectioned into four sets of 40-µm-thick sections spanning the entire brain, and immunofluorescent labeling was performed as described above. eGFP-expressing cell bodies were counted in one full set of sections for each brain.

Digital image processing

Images of whole embryos and adult organs were collected on a Zeiss SteREO Lumar.V12 stereomicroscope (Carl Zeiss Microscopy, Thornwood, NY). Immunoperoxidase-labeled sections were imaged on a Zeiss Axio Imager Z2. Images of fluorescently labeled sections were collected on a Zeiss LSM 710 or 780 inverted confocal microscope. After *z*-stacks were converted to maximum intensity projections using Zen 2012 Black Software (Carl Zeiss), the images were modified only by adjusting brightness and contrast to optimize the full dynamic range of the fluorescence signal of the entire image using Photoshop software (Adobe Systems). The location of imaged neurons was determined by reference to a mouse brain atlas (Paxinos and Franklin, 2013). Adult brain tissue cleared by PACT was imaged on a Zeiss LSM 780 microscope, and images of locus coeruleus cell bodies were compiled into three-dimensional structures and processed (background subtraction and attenuation correction) using Imaris Software (Bitplane). Images of axon fibers from PACT-cleared tissue were also acquired on a Zeiss LSM 780, after which images were first processed with ImageJ software (NIH) by simply multiplying the image times itself to increase the fluorescence signal above the background and then run through a smoothing filter before being imported into Imaris (Bitplane) where 3D volume rendering was performed. E12.5 embryos cleared by PACT were imaged on a Zeiss LSM 780, and images were imported into Imaris for cropping and 3D rendering.

Acknowledgements

We thank D. D'Agostin, G. Jones, G. Keeley, and K. Smith for technical assistance. We also thank F. Stewart (Technische Universität Dresden) and R. Tsien (UC San Diego) for DNA constructs. The National Institute of Environmental Health Sciences vivarium and knockout mouse core provided valuable support. We thank Georgia Alexander and members of the Jensen lab for helpful discussion.

Competing interests

The authors declare no competing or financial interests.

Author contributions

N.W.P. and P.J. designed the targeting vectors. N.W.P. generated all new mouse lines. N.W.P., I.Y.E., S.D.R. and P.J. characterized the new lines. J.d.M. provided unpublished reagents. N.W.P. and C.J.T. collected and processed digital images. N.W.P. and P.J. wrote the manuscript with input from other co-authors.

Funding

This research was supported by the Intramural Research Program of the US National Institutes of Health, National Institute of Environmental Health Sciences (ZIA-ES-102805). Deposited in PMC for release after 12 months.

Supplementary information

Supplementary information available online at
http://dev.biologists.org/lookup/suppl/doi:10.1242/dev.129981/-/DC1

References

Anastassiadis, K., Fu, J., Patsch, C., Hu, S., Weidlich, S., Duerschke, K., Buchholz, F., Edenhofer, F. and Stewart, A. F. (2009). Dre recombinase, like Cre, is a highly efficient site-specific recombinase in E. coli, mammalian cells and mice. *Dis. Model. Mech.* **2**, 508-515.

Andrews, B. J., Proteau, G. A., Beatty, L. G. and Sadowski, P. D. (1985). The FLP recombinase of the 2µ circle DNA of yeast: interaction with its target sequences. *Cell* **40**, 795-803.

Awatramani, R., Soriano, P., Rodriguez, C., Mai, J. J. and Dymecki, S. M. (2003). Cryptic boundaries in roof plate and choroid plexus identified by intersectional gene activation. *Nat. Genet.* **35**, 70-75.

Bang, S. J., Jensen, P., Dymecki, S. M. and Commons, K. G. (2012). Projections and interconnections of genetically defined serotonin neurons in mice. *Eur. J. Neurosci.* **35**, 85-96.

Chandler, D. J. and Waterhouse, B. D. (2012). Evidence for broad versus segregated projections from cholinergic and noradrenergic nuclei to functionally and anatomically discrete subregions of prefrontal cortex. *Front. Behav. Neurosci.* **6**, 20.

Chandler, D. J., Lamperski, C. S. and Waterhouse, B. D. (2013). Identification and distribution of projections from monoaminergic and cholinergic nuclei to functionally differentiated subregions of prefrontal cortex. *Brain Res.* **1522**, 38-58.

Chandler, D. J., Gao, W.-J. and Waterhouse, B. D. (2014). Heterogeneous organization of the locus coeruleus projections to prefrontal and motor cortices. *Proc. Natl. Acad. Sci. USA* **111**, 6816-6821.

Development (2015) 142, 4385-4393 doi:10.1242/dev.129981

Chung, K., Wallace, J., Kim, S.-Y., Kalyanasundaram, S., Andalman, A. S., Davidson, T. J., Mirzabekov, J. J., Zalocusky, K. A., Mattis, J., Denisin, A. K. et al. (2013). Structural and molecular interrogation of intact biological systems. *Nature* **497**, 332-337.

Cocas, L. A., Miyoshi, G., Carney, R. S. E., Sousa, V. H., Hirata, T., Jones, K. R., Fishell, G., Huntsman, R. R. and Corbin, J. G. (2009). Emx1-lineage progenitors differentially contribute to neural diversity in the striatum and amygdala. *J. Neurosci.* **29**, 15933-15946.

Duan, B., Cheng, L., Bourane, S., Britz, O., Padilla, C., Garcia-Campmany, L., Krashes, M., Knowlton, W., Velasquez, T., Ren, X. et al. (2014). Identification of spinal circuits transmitting and gating mechanical pain. *Cell* **159**, 1417-1432.

Dymecki, S. M. and Tomasiewicz, H. (1998). Using Flp-recombinase to characterize expansion of Wnt1-expressing neural progenitors in the mouse. *Dev. Biol.* **201**, 57-65.

Ertürk, A., Becker, K., Jährling, N., Mauch, C. P., Hojer, C. D., Egen, J. G., Hellal, F., Bradke, F., Sheng, M. and Dodt, H.-U. (2012). Three-dimensional imaging of solvent-cleared organs using 3DISCO. *Nat. Protoc.* **7**, 1983-1995.

Farago, A. F., Awatramani, R. B. and Dymecki, S. M. (2006). Assembly of the brainstem cochlear nuclear complex is revealed by intersectional and subtractive genetic fate maps. *Neuron* **50**, 205-218.

Fenno, L. E., Mattis, J., Ramakrishnan, C., Hyun, M., Lee, S. Y., He, M., Tucciarone, J., Selimbeyoglu, A., Berndt, A., Grosenick, L. et al. (2014). Targeting cells with single vectors using multiple-feature Boolean logic. *Nat. Methods* **11**, 763-772.

Friedrich, G. and Soriano, P. (1991). Promoter traps in embryonic stem cells: a genetic screen to identify and mutate developmental genes in mice. *Genes Dev.* **5**, 1513-1523.

George, S. H. L., Gertsenstein, M., Vintersten, K., Korets-Smith, E., Murphy, J., Stevens, M. E., Haigh, J. J. and Nagy, A. (2007). Developmental and adult phenotyping directly from mutant embryonic stem cells. *Proc. Natl. Acad. Sci. USA* **104**, 4455-4460.

Gong, S., Doughty, M., Harbaugh, C. R., Cummins, A., Hatten, M. E., Heintz, N. and Gerfen, C. R. (2007). Targeting Cre recombinase to specific neuron populations with bacterial artificial chromosome constructs. *J. Neurosci.* **27**, 9817-9823.

Hama, H., Kurokawa, H., Kawano, H., Ando, R., Shimogori, T., Noda, H., Fukami, K., Sakaue-Sawano, A. and Miyawaki, A. (2011). Scale: a chemical approach for fluorescence imaging and reconstruction of transparent mouse brain. *Nat. Neurosci.* **14**, 1481-1488.

Hermann, M., Stillhard, P., Wildner, H., Seruggia, D., Kapp, V., Sanchez-Iranzo, H., Mercader, N., Montoliu, L., Zeilhofer, H. U. and Pelczar, P. (2014). Binary recombinase systems for high-resolution conditional mutagenesis. *Nucleic Acids Res.* **42**, 3894-3907.

Holets, V. R., Hökfelt, T., Rökaeus, A., Terenius, L. and Goldstein, M. (1988). Locus coeruleus neurons in the rat containing neuropeptide Y, tyrosine hydroxylase or galanin and their efferent projections to the spinal cord, cerebral cortex and hypothalamus. *Neuroscience* **24**, 893-906.

Huang, Z. J. (2014). Toward a genetic dissection of cortical circuits in the mouse. *Neuron* **83**, 1284-1302.

Jensen, P. and Dymecki, S. M. (2014). Essentials of recombinase-based genetic fate mapping in mice. *Methods Mol. Biol.* **1092**, 437-454.

Jensen, P., Farago, A. F., Awatramani, R. B., Scott, M. M., Deneris, E. S. and Dymecki, S. M. (2008). Redefining the serotonergic system by genetic lineage. *Nat. Neurosci.* **11**, 417-419.

Kato, S., Kuramochi, M., Takasumi, K., Kobayashi, K., Inoue, K.-i., Takahara, D., Hitoshi, S., Ikenaka, K., Shimada, T., Takada, M. et al. (2011). Neuron-specific gene transfer through retrograde transport of lentiviral vector pseudotyped with a novel type of fusion envelope glycoprotein. *Hum. Gene Ther.* **22**, 1511-1523.

Ke, M.-T., Fujimoto, S. and Imai, T. (2013). SeeDB: a simple and morphology-preserving optical clearing agent for neuronal circuit reconstruction. *Nat. Neurosci.* **16**, 1154-1161.

Kim, J. C., Cook, M. N., Carey, M. R., Shen, C., Regehr, W. G. and Dymecki, S. M. (2009). Linking genetically defined neurons to behavior through a broadly applicable silencing allele. *Neuron* **63**, 305-315.

Kimmel, R. A., Turnbull, D. H., Blanquet, V., Wurst, W., Loomis, C. A. and Joyner, A. L. (2000). Two lineage boundaries coordinate vertebrate apical ectodermal ridge formation. *Genes Dev.* **14**, 1377-1389.

Lewandoski, M., Meyers, E. N. and Martin, G. R. (1997). Analysis of Fgf8 gene function in vertebrate development. *Cold Spring Harb. Symp. Quant. Biol.* **62**, 159-168.

Lundgren, O., Jodal, M., Jansson, M., Ryberg, A. T. and Svensson, L. (2011). Intestinal epithelial stem/progenitor cells are controlled by mucosal afferent nerves. *PLoS ONE* **6**, e16295.

Madisen, L., Zwingman, T. A., Sunkin, S. M., Oh, S. W., Zariwala, H. A., Gu, H., Ng, L. L., Palmiter, R. D., Hawrylycz, M. J., Jones, A. R. et al. (2010). A robust and high-throughput Cre reporting and characterization system for the whole mouse brain. *Nat. Neurosci.* **13**, 133-140.

Madisen, L., Garner, A. R., Shimaoka, D., Chuong, A. S., Klapoetke, N. C., Li, L., van der Bourg, A., Niino, Y., Egolf, L., Monetti, C. et al. (2015). Transgenic mice for intersectional targeting of neural sensors and effectors with high specificity and performance. *Neuron* **85**, 942-958.

Matthies, H. J. G., Han, Q., Shields, A., Wright, J., Moore, J. L., Winder, D. G., Galli, A. and Blakely, R. D. (2009). Subcellular localization of the antidepressant-sensitive norepinephrine transporter. *BMC Neurosci.* **10**, 65.

McCall, J. G., Al-Hasani, R., Siuda, E. R., Hong, D. Y., Norris, A. J., Ford, C. P. and Bruchas, M. R. (2015). CRH engagement of the locus coeruleus noradrenergic system mediates stress-induced anxiety. *Neuron* **87**, 605-620.

Miller, M. A., Kolbe, P. E., Leverenz, J. B., Peskind, E. R. and Raskind, M. A. (1999). Preservation of noradrenergic neurons in the locus coeruleus that coexpress galaning mRNA in Alzheimer's disease. *J. Neurochem.* **73**, 2028-2036.

Miyoshi, G., Hjerling-Leffler, J., Karayannis, T., Sousa, V. H., Butt, S. J. B., Battiste, J., Johnson, J. E., Machold, R. P. and Fishell, G. (2010). Genetic fate mapping reveals that the caudal ganglionic eminence produces a large and diverse population of superficial cortical interneurons. *J. Neurosci.* **30**, 1582-1594.

Niwa, H., Yamamura, K. and Miyazaki, J. (1991). Efficient selection for high-expression transfectants with a novel eukaryotic vector. *Gene* **108**, 193-199.

O'Gorman, S. (2005). Second branchial arch lineages of the middle ear of wild-type and Hoxa2 mutant mice. *Dev. Dyn.* **234**, 124-131.

Olpe, H.-R. and Steinmann, M. (1991). Responses of locus coeruleus neurons to neuropeptides. *Prog. Brain Res.* **88**, 241-248.

Paxinos, G. and Franklin, K. B. J. (2013). *The Mouse Brain in Stereotaxic Coordinates*. San Diego: Academic Press.

Poulin, J.-F., Zou, J., Drouin-Ouellet, J., Kim, K.-Y., Cicchetti, F. and Awatramani, R. B. (2014). Defining midbrain dopaminergic neuron diversity by single-cell gene expression profiling. *Cell Rep.* **9**, 930-943.

Raymond, C. S. and Soriano, P. (2007). High-efficiency FLP and ϕC31 site-specific recombination in mammalian cells. *PLoS ONE* **2**, e162.

Renier, N., Wu, Z., Simon, D. J., Yang, J., Ariel, P. and Tessier-Lavigne, M. (2014). iDISCO: a simple, rapid method to immunolabel large tissue samples for volume imaging. *Cell* **159**, 896-910.

Robertson, S. D., Plummer, N. W., de Marchena, J. and Jensen, P. (2013). Developmental origins of central norepinephrine neuron diversity. *Nat. Neurosci.* **16**, 1016-1023.

Rodriguez, C. I., Buchholz, F., Galloway, J., Sequerra, R., Kasper, J., Ayala, R., Stewart, A. F. and Dymecki, S. M. (2000). High-efficiency deleter mice show that FLPe is an alternative to Cre-loxP. *Nat. Genet.* **25**, 139-140.

Sakamoto, M., Ieki, N., Miyoshi, G., Mochimaru, D., Miyachi, H., Imura, T., Yamaguchi, M., Fishell, G., Mori, K., Kageyama, R. et al. (2014). Continuous postnatal neurogenesis contributes to formation of the olfactory bulb neural circuits and flexible olfactory associative learning. *J. Neurosci.* **34**, 5788-5799.

Sauer, B. (1993). Manipulation of transgenes by site-specific recombination: use of Cre recombinase. *Methods Enzymol.* **225**, 890-900.

Sauer, B. and McDermott, J. (2004). DNA recombination with a heterospecific Cre homolog identified from comparison of the pac-c1 regions of P1-related phages. *Nucleic Acids Res.* **32**, 6086-6095.

Schwarz, L. A., Miyamachi, K., Gao, X. J., Beier, K. T., Weissbourd, B., DeLoach, K. E., Ren, J., Ibanes, S., Malenka, R. C., Kremer, E. J. et al. (2015). Viral-genetic tracing of the input–output organization of a central noradrenaline circuit. *Nature* **524**, 88-92.

Sciolino, N. R., Smith, J. M., Stranahan, A. M., Freeman, K. G., Edwards, G. L., Weinshenker, D. and Holmes, P. V. (2015). Galanin mediates features of neural and behavioral stress resilience afforded by exercise. *Neuropharmacology* **89**, 255-264.

Sevcik, J., Finta, E. P. and Illes, P. (1993). Galanin receptors inhibit the spontaneous firing of locus coeruleus neurones and interact with μ-opioid receptors. *Eur. J. Pharmacol.* **230**, 223-230.

Soudais, C., Laplace-Builhe, C., Kissa, K. and Kremer, E. J. (2001). Preferential transduction of neurons by canine adenovirus vectors and their efficient retrograde transport in vivo. *FASEB J.* **15**, 2283-2285.

Sternberg, N. and Hamilton, D. (1981). Bacteriophage P1 site-specific recombination. I. Recombination between loxP sites. *J. Mol. Biol.* **150**, 467-486.

Xu, Z.-Q., Shi, T.-J. S. and Hökfelt, T. (1998). Galanin/GMAP- and NPY-like immunoreactivities in locus coeruleus and noradrenergic nerve terminals in the hippocampal formation and cortex with notes on the galanin-R1 and -R2 receptors. *J. Comp. Neurol.* **392**, 227-251.

Yamamoto, M., Shook, N. A., Kanisicak, O., Yamamoto, S., Wosczyna, M. N., Camp, J. R. and Goldhamer, D. J. (2009). A multifunctional reporter mouse line for Cre- and FLP-dependent lineage analysis. *Genesis* **47**, 107-114.

Yang, B., Treweek, J. B., Kulkarni, R. P., Deverman, B. E., Chen, C.-K., Lubeck, E., Shah, S., Cai, L. and Gradinaru, V. (2014). Single-cell phenotyping within transparent intact tissue through whole-body clearing. *Cell* **158**, 945-958.

Zinyk, D. L., Mercer, E. H., Harris, E. Anderson, D. J. and Joyner, A. L. (1998). Fate mapping of the mouse midbrain–hindbrain constriction using a site-specific recombination system. *Curr. Biol.* **8**, 665-672.

Zufferey, R., Donello, J. E., Trono, T. J. and Hope, T. J. (1999). Woodchuck hepatitis virus posttranscriptional regulatory element enhances expression of transgenes delivered by retroviral vectors. *J. Virol.* **73**, 2886-2892.

SUPPLEMENTARY FIGURES

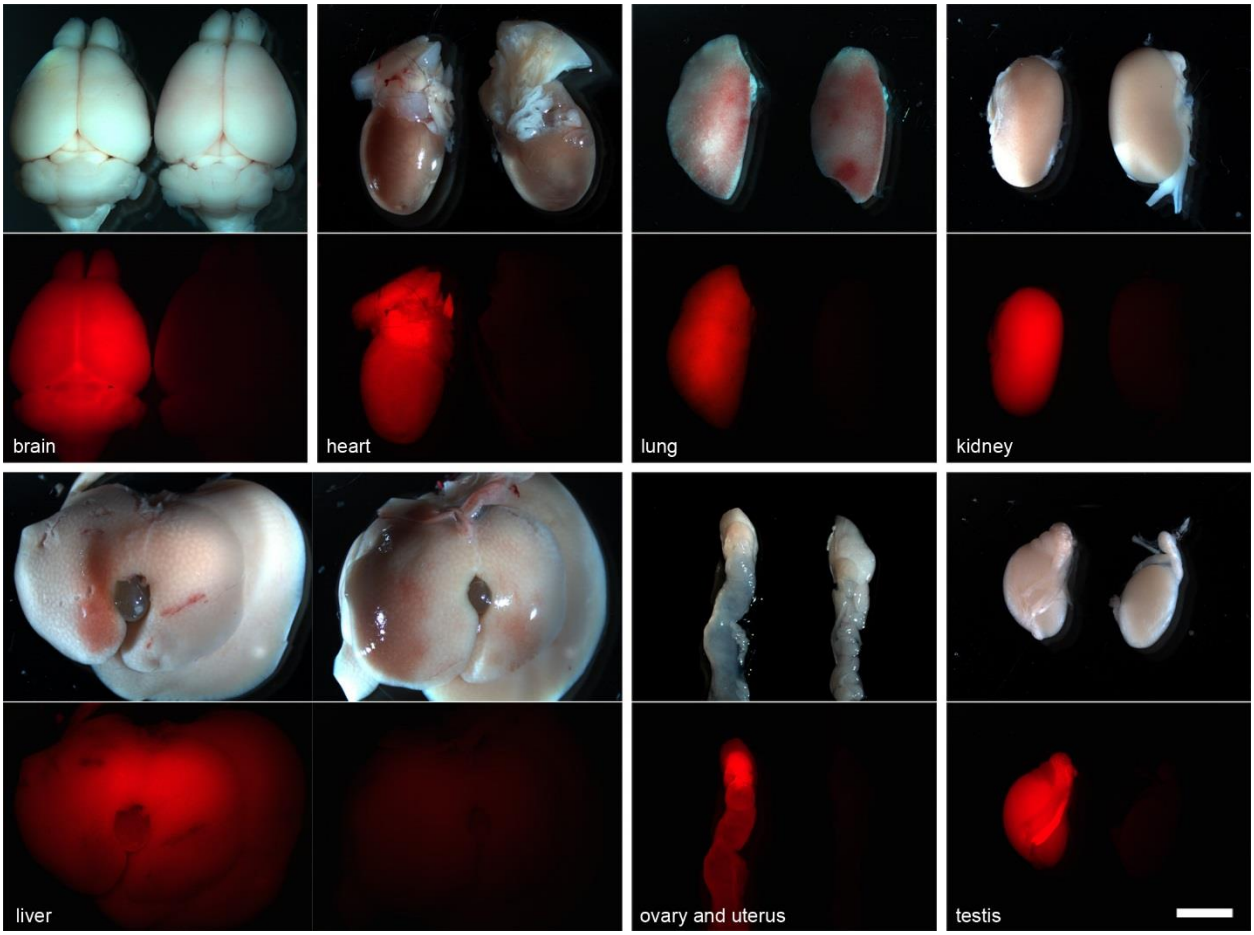

Fig. S1. Cells in a wide variety of organs and tissues can be labeled by *RC::RFLTG* and its derivative alleles.

Ubiquitous activity of the CAG promoter in *RC::RFLTG* and its derivative alleles in a variety of organs is demonstrated by tdTomato fluorescence in 6-7 week old *CAG-Dre; ACTB-Flpe; RC::RFLTG* mice (left of each pair of organs, n=10). No fluorescence was seen in control organs (right of each pair, n=6) due to the presence of transcriptional stop cassettes (control brain, *RC::RFLTG*; other organs, *RC::RLTG*). **Top two rows, left to right:** Brain, heart, lung, kidney. **Bottom two rows, left to right:** liver, ovary and uterus, testis. Images show native fluorescence. Scale bar: 5 mm.

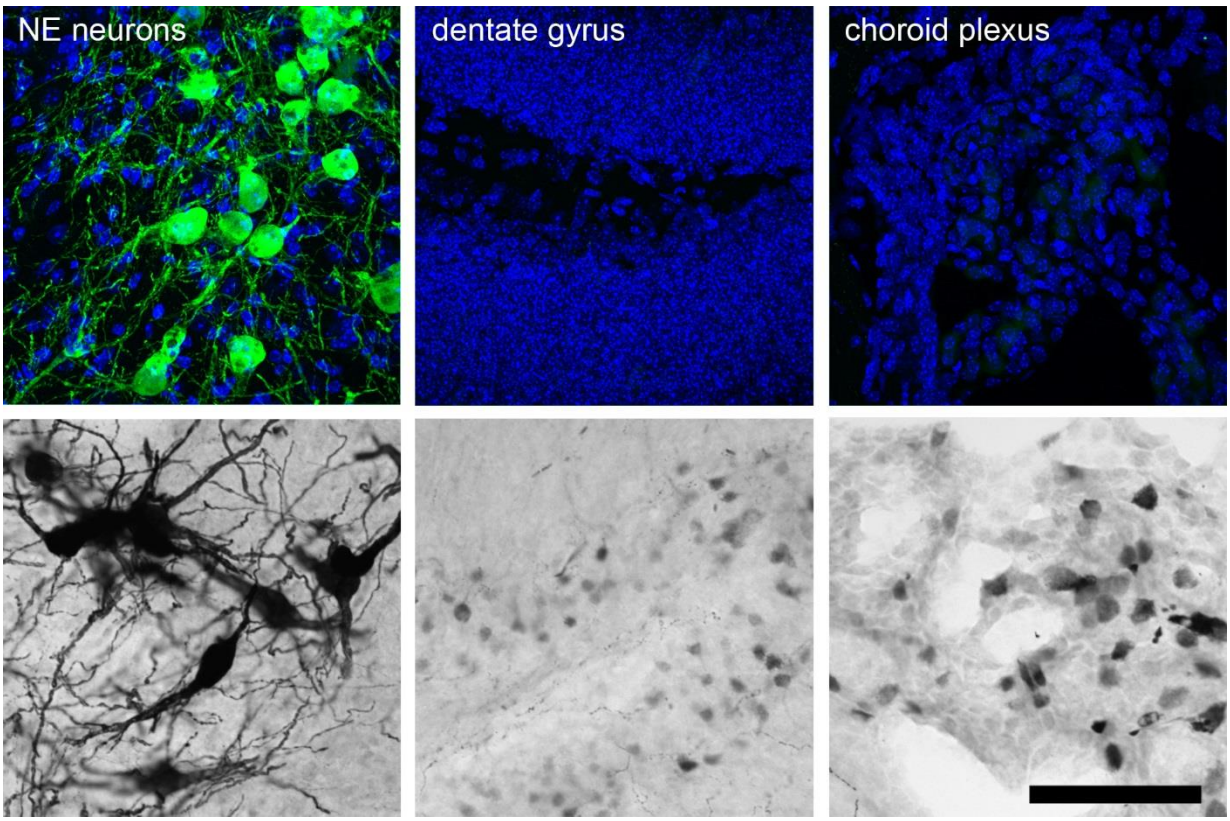

Fig. S2. eGFP expressed from *RC::RFLTG* after recombination is readily distinguished from very low level expression occurring in the absence of recombinases in choroid plexus and hippocampus.

eGFP expression in the brain of *En1^{Dre}; Dbh^{Flpo}; Gal-Cre; RC::RFLTG* mice was detected by immunohistochemistry using either a fluorescently labeled secondary antibody (top, n=10) or a horseradish peroxidase-coupled secondary antibody and fifteen minute incubation with the Vector SG chromogen for maximal staining (bottom, n=4). Noradrenergic (NE) neurons that have expressed all three recombinases are readily detected in the fluorescently labeled sample (top left), but eGFP is virtually undetectable in fluorescently labeled dentate gyrus (top center) and choroid plexus (top right) cells that have not expressed recombinases. Nuclear DAPI

fluorescence (blue) shows the presence of cells that are not otherwise labeled. Following the full fifteen minutes of chromogen precipitation, the staining is saturated in noradrenergic neurons (bottom left). Chromogen staining is much less dense in dentate gyrus (bottom center) and choroid plexus (bottom right) cells, allowing them to be readily distinguished from recombinase-expressing neurons (bottom left). Scale bar: 92 µm (top row) or 100 µm (bottom row).

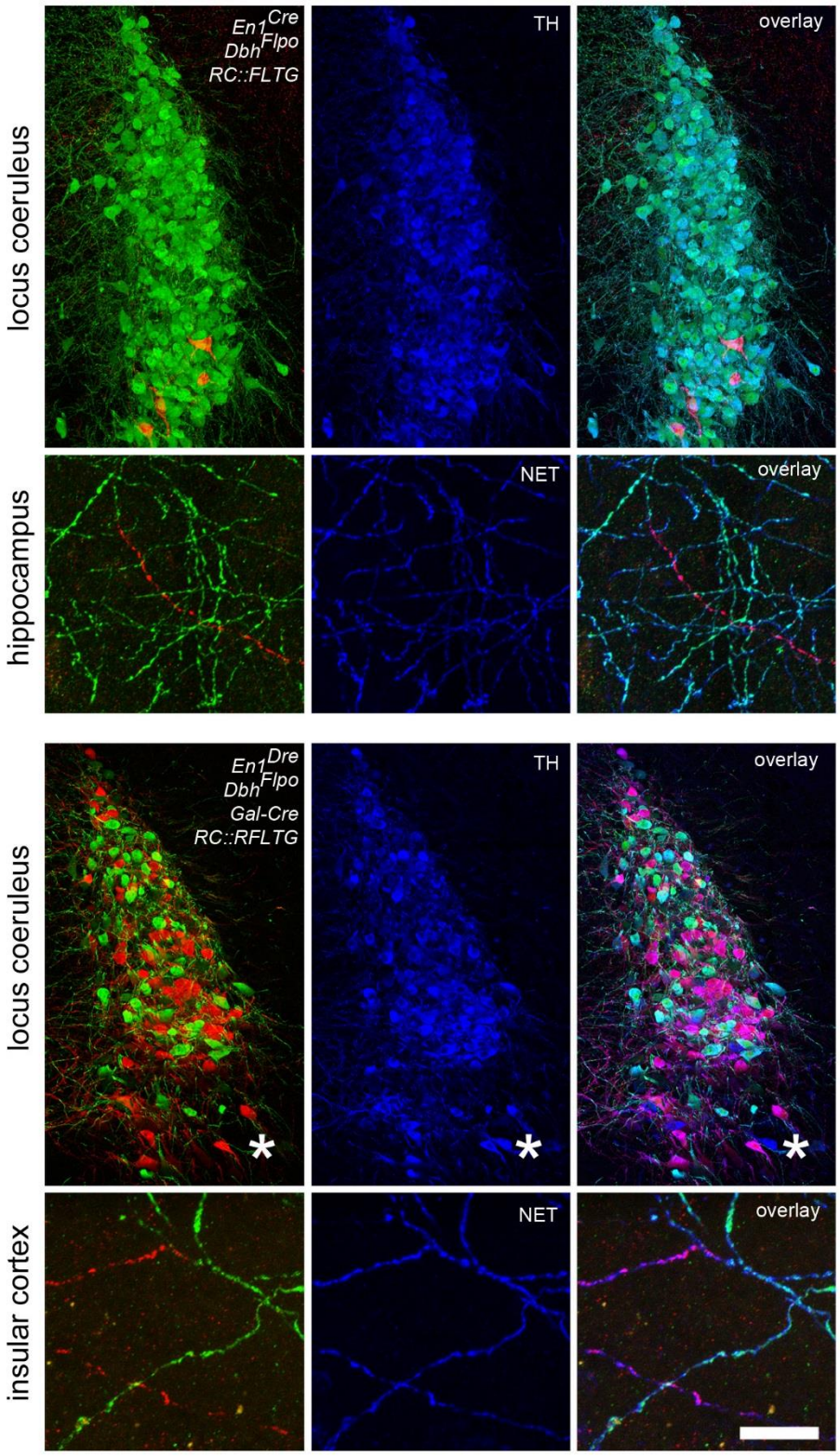

Fig. S3: Immunostaining with anti-tryosine hydroxylase and anti-norepinephrine transporter antibodies confirms that intersectional crosses with *RC::FLTG* and *RC::RFLTG* efficiently label noradrenergic neurons.

Top row: In *En1^{Cre}; Dbh^{Flpo}; RC::FLTG* brain (n=4), noradrenergic neurons (locus coeruleus shown) with history of *En1* expression are labeled with eGFP, while those originating outside the *En1* expression domain are labeled with tdTomato. Co-labeling with an antibody against tyrosine hydroxylase (TH), an enzyme required for norepinephrine synthesis, confirms that recombination of *RC::FLTG* by these driver alleles efficiently labels the entire locus coeruleus. **Second row:** At projection target sites (hippocampus shown), co-labeling with an antibody against the norepinephrine transporter (NET) demonstrates that eGFP- and tdTomato-labeled axons originate from noradrenergic neurons. **Third row:** In *En1^{Dre}; Dbh^{Flpo}; Gal-Cre; RC::RFLTG* brain (n=4), only locus coeruleus neurons originating from the *En1* expression domain are labeled with eGFP (*Gal-Cre*-expressing) or tdTomato (*Gal-Cre*-negative). The very few locus coeruleus neurons originating outside the *En1* domain are labeled with anti-TH antibody, but neither eGFP nor tdTomato (blue neuron at left of asterisk). **Fourth Row:** At target sites of locus coeruleus projections (insular cortex shown), co-labeling with ant-NET demonstrates that eGFP- and tdTomato-labeled axons originate from noradrenergic neurons of the locus coeruleus complex. Images show immunofluorescence. Scale bar: 120 μm (locus coeruleus) or 20 μm (axons).

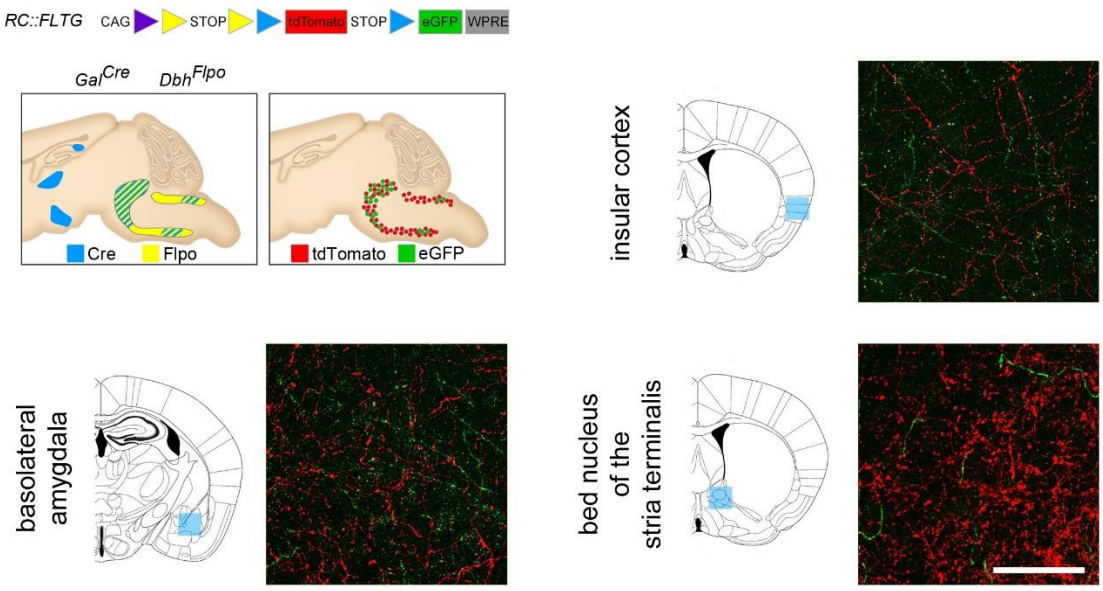

Fig. S4: Axons from all *Gal-Cre*-expressing and *Gal-Cre*-negative noradrenergic neurons can be labeled using a dual-recombinase responsive indicator allele.

In *Gal-Cre; Dbh*^{Flpo}*; RC::FLTG* brain (n=4), *Gal-Cre*-expressing (eGFP-labeled) and *Gal-Cre*-negative (tdTomato-labeled) axons can be observed at target sites of noradrenergic projections. However, at sites which receive projections originating both within and outside the LC complex (e.g. insular cortex, amygdala, bed nucleus of the stria terminalis), *Gal-Cre*-expressing and *Gal-Cre*-negative axons from the LC complex cannot be distinguished from those originating in other noradrenergic subpopulations. Images show immunofluorescence. Scale bar: 50 μm

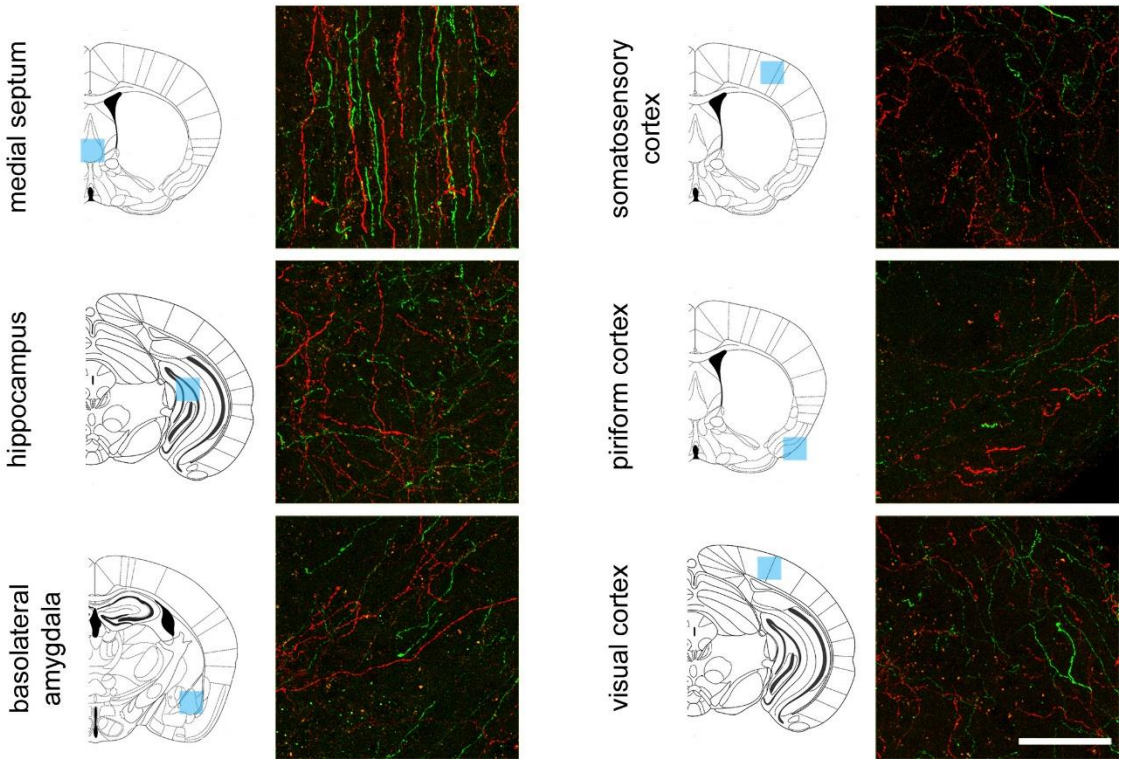

Fig. S5: Axons from *Gal-Cre*-expressing and *Gal-Cre*-negative neurons in the LC complex project to the same forebrain target regions.

In *En1*^{Dre}*; Dbh*^{Flpo}*; Gal-Cre; RC::RFLTG* quadruple heterozygous brain (n=10), eGFP-labeled (*Gal-Cre*-expressing) and tdTomato-labeled (*Gal-Cre*-negative) axons are observed intermingled at representative forebrain target sites. The blue boxes on the line diagrams show the approximate location of the imaged axons in coronal sections. Images show immunofluorescence. Scale bar: 50 µm

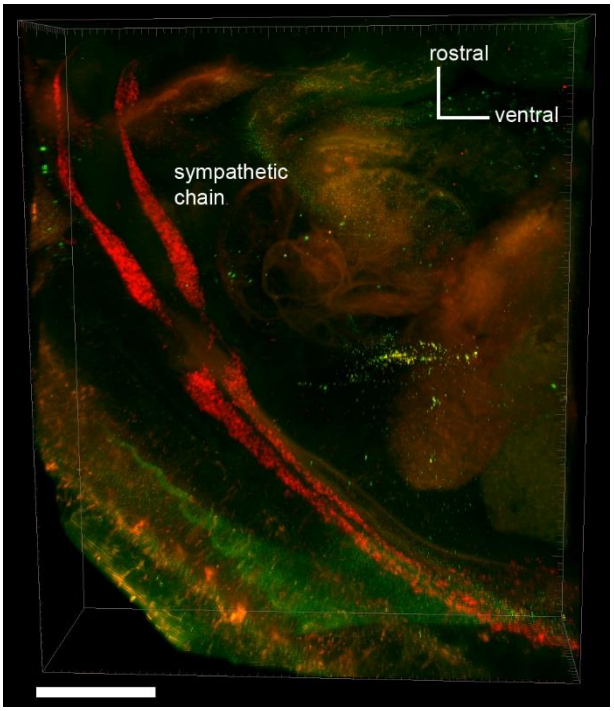

Fig. S6. Labeled cells can be observed within intact embryos cleared by the passive clarity technique.

tdTomato-labeled sympathetic ganglia are visible in the thoracic region of an E12.5 *Dbh*^{Flpo}*; RC::FLTG* double heterozygous embryo (n=2) cleared with PACT. The intact shape and relative position of the bilaterally symmetric sympathetic chains can be clearly discerned. Image shows immunofluorescence. Scale bar: 600 µm.

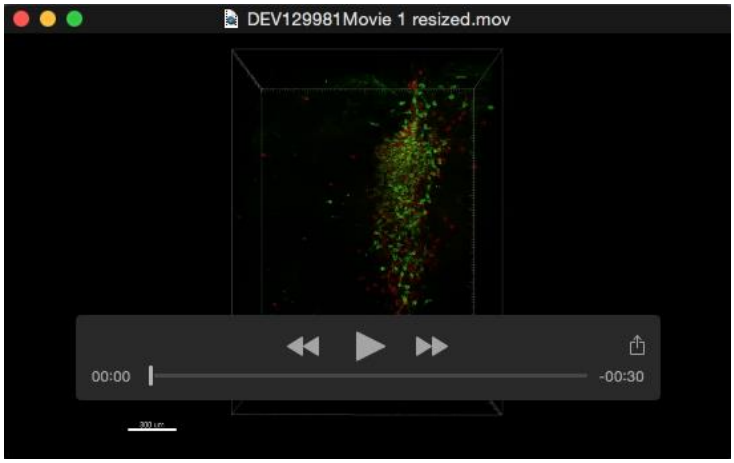

Movie 1. The intact structure of the locus coeruleus and dorsal subcoeruleus, and the spatial relationship of two subpopulations labeled with eGFP and tdTomato expressed from *RC::RFLTG*, are revealed in brain cleared by the passive clarity technique.

After PACT clearing and immunostaining of *En1*^{Dre}; *Dbh*^{Flpo}; *Gal-Cre*; *RC::RFLTG brain*, the morphology of the LC complex, divided into *Gal-Cre*-expressing (eGFP) and *Gal-Cre*-negative (tdTomato) subpopulations, can be observed. The neurons form a single, unbroken continuum extending from the densely packed locus coeruleus to the more loosely arranged subcoeruleus (see Fig. 5). *Gal-Cre*-expressing and *Gal-Cre*-negative noradrenergic neurons are intermingled throughout the structure, and a very few *Gal-Cre*-negative cells are widely displaced from the main body of neurons along the mediolateral axis. At the beginning of the movie, the rostral aspect of the population faces forward with the dorsal surface uppermost.

SUPPLEMENTARY MATERIALS AND METHODS

Generation of *RC::RFLTG* targeting vector

To facilitate insertion of three His3-SV40 transcriptional stop cassettes into the targeting vector, we first generated a version of pBS302 (Sauer, 1993) which lacks the *Mfe*I site in the SV40 poly(A) cassette. pBS302 was digested with *Mfe*I, the single strand overhang filled in, and the plasmid re-ligated. This modified pBS302 served as template for production of all three stop cassettes, as described below.

For the stop cassette following the tdTomato cDNA, the His3-Sv40 stop sequence was amplified with primers 5'-GACTAGTAGCTAGCAATTGTCGGGGACACCAAATATGGCGATC and 5'-GACTAGGAATTCTGATCATAGGTCCCTCGACCTGCAGCCCAAGC which contain *Eco*RI, *Mfe*I, and *Bcl*I sites. This PCR product was digested with *Eco*RI and *Mfe*I, and cloned into the *Eco*RI site of pRSET-tdTomato (Shaner et al., 2004). The tdTomato-stop was isolated by digestion with *Nhe*I and *Bcl*I and cloned into pL452 (Liu et al., 2003) digested with the same restriction enzymes. The resulting plasmid, ploxtdTomato, has loxP sites flanking tdTomato, His3-SV40 stop cassette, and bovine growth hormone (bGH) poly(A) cassette.

pCAG-GFP (Matsuda and Cepko, 2004), which has an enhanced green fluorescent protein gene controlled by CAG promoter (Niwa et al., 1991), was digested with *Not*I. The single-strand overhang was filled-in, and the plasmid was re-ligated to replace the *Not*I site with an *Fse*I site between the eGFP cDNA and β-globin polyadenylation cassette. ploxtdTomato was digested with *Spe*I and the single-strand overhang was filled in to generate a blunt end. The linearized plasmid was then digested with *Eco*RI, and the loxP-flanked tdTomato-His3-SV40 stop-bGH poly(A) was cloned between the *Sma*I and *Eco*RI sites of the modified pCAG-GFP to generate pCAG-loxTloxG.

The FRT-flanked His3-SV40 stop cassette was amplified from the modified pBS302 using primers 5'- GACTAGGAATTCGAAGTTCCTATTCTCTAGAAAGTATAGGAACTTCTCGG GGACACCAAATATGGCGATC and 5'- GACTAGTAGCTAGCAATTGATGCATGAAGTTCC TATACTTTCTAGAGAATAGGAACTTCTAGGTCCCTCGACCTGCAGCCCAAGC. The primers contain FRT sites (underlined) and *Eco*RI, *Mfe*I and *Nsi*I sites for subsequent cloning. The rox-flanked stop cassette was amplified with primers 5'-GACTGAATTCTAACTTTAAATAATGCCAAT TATTTAAAGTTATCGGGGACACCAAATATGGCGATC and 5'-GACTGACTCAATTGTAACTTTA AATAATTGGCATTATTTAAAGTTATAGGTCCCTCGACCTGCAGCCCAAGC. The primers contain rox sites (underlined) and *Eco*RI and *Mfe*I sites for cloning. The FRT-flanked and rox-flanked cassettes were digested with *Eco*RI and *Mfe*I and cloned sequentially into the *Eco*RI site of the pCAG-loxTloxG to generate pCAG-RFLTG.

A *Spe*I-*Pac*I-*Avr*II linker was generated by annealing oligonucleotides with the sequence 5'-CTAGTTTAATTAAC and 5'-CTAGGTTAATTAAA and cloned into the *Spe*I site upstream of the CAG promoter. An *Eco*RI-*Mlu*I-*Mfe*I linker was generated by annealing 5'- AATTCACGCGTC and 5'- AATTGACGCGTG and cloned into the *Eco*RI site downstream of the CAG promoter. Finally, the CAG promoter, STOP cassettes, and fluorophore cDNAs were all isolated in a single fragment by digestion with *Pac*I and *Fse*I and cloned into pAi9 (Madisen et al., 2010) digested with the same two enzymes to generate the *Gt(ROSA)26Sor* targeting vector, pRC-RFLTG (p**R**osa-**C**AG-**r**ox-**F**RT-**l**oxP-td**T**omato-e**G**FP). The digested fragment of pAi9 provided the woodchuck hepatitis virus posttranscriptional regulatory element (WPRE) (Zufferey at al., 1999) and bGH poly(A) cassette that follow the eGFP cDNA, the 5' and 3' homology to the *Gt(ROSA)26Sor* locus (Friedrich and Soriano, 1991), attB/attP-flanked Neo cassette, and diphtheria toxin (DTA) cassette for negative selection in embryonic stem cells. The WPRE is not expected to have any effect on expression of tdTomato, because a stop cassette is

located between the tdTomato and eGFP cDNAs. pRC-RFLTG has unique *Kpn*I, *Pac*I, *Mlu*I, *Fse*I, and *Asc*I sites to facilitate additional modification. For transformation of ES cells, the vector was linearized with *Kpn*I.

PACT tissue clearing and immunofluorescence

For the passive clarity technique, we followed the previously published protocol (Yang et al., 2014). Mice were perfused and brains post-fixed overnight in 4% PFA as described above. After rinsing in PBS, brains were cut into four 3 mm-thick coronal slices using a brain matrix. The slices were embedded in 4% polyacrylamide gel (A4P0) and lipids were extracted by incubation in 8% SDS at 37 °C for four days. Cleared brain slices were washed five times in PBS for 1 hour each rinse at room temperature and then washed overnight in PBS with 0.01% sodium azide. Prior to addition of antibodies, slices were incubated in PBS with 0.1% Triton X-100 (PBST), 5% donkey serum and 0.01% sodium azide for 24 hours at room temperature. The slices were then incubated in PBST with primary antibodies, 2% donkey serum, and 0.01% sodium azide on an orbital shaker at room temperature. The rabbit anti-dsRed antibody was used at 1:500 dilution and the chicken anti-GFP at 1:1000. The buffer and antibodies were replaced with fresh solution after three days, and after a total of five days incubation, the slices were rinsed in PBST and washed overnight in PBST with 0.1% sodium azide. The following day, the slices were washed 5 more times in PBST for one hour each wash and then incubated at room temperature in PBST with Alexa Fluor 568 donkey anti-rabbit F(ab')2 fragments (1:500), Alexa Fluor 488 donkey anti-chicken F(ab')2 fragments (1:500), 2% donkey serum, and 0.01% sodium azide. Buffer and antibodies were replaced with fresh solution after three days and the incubation continued for two more days. The slices were washed five times in PBST for one hour each and

then washed overnight in PBS at 4 °C. The following day, the slices were transferred to RIMS (Yang et al., 2014). After overnight incubation at 4 °C, the slices were mounted in fresh RIMS between two coverslips separated by a 3 mm iSpacer (SunJin Lab Company, Hsinchu City, Taiwan) and imaged. E12.5 embryos were fixed by immersion overnight in 4% PFA in PBS, embedded in A4P0, and cleared in 8% SDS for 14 hours at room temperature. After the embryos were rinsed in PBS, immunofluorescent labeling and mounting in RIMS was performed as described for brain slices.

SUPPLEMENTARY REFERENCES

Friedrich, G., and Soriano, P. (1991). Promoter traps in embryonic stem cells: a genetic screen to identify and mutate developmental genes in mice. *Genes Dev.* **5**, 1513-1523.

Liu, P., Jenkins, N. A., and Copeland, N. G. (2003). A highly efficient recombineering-based method for generating conditional knockout mutations. *Genome Res.* **13**, 476-484.

Madisen, L., Zwingman, T. A., Sunkin, S. M., Oh, S. W., Zariwala, H. A., Gu, H., Ng, L. L., Palmiter, R. D., Hawrylycz, M. J., Jones, A. R., Lein, E. S., and Zeng, H. (2010). A robust and high-throughput Cre reporting and characterization system for the whole mouse brain. *Nat. Neurosci.* **13**, 133-140.

Matsuda, T., and Cepko, C. L. (2004). Electroporation and RNA interference in the rodent retina in vivo and in vitro. *Proc. Natl. Acad. Sci. USA* **101**, 16-22.

Niwa, H., Yamamura, K., and Miyazaki, J. (1991). Efficient selection for high-expression transfectants with a novel eukaryotic vector. *Gene* **108**, 193-199.

Sauer, B. (1993). Manipulation of transgenes by site-specific recombination: use of Cre recombinase. *Methods Enzymol.* **225**, 890-900.

Shaner, N. C., Campbell, R. E., Steinbach, P. A., Giepmans, B. N., Palmer, A. E., and Tsien, R. Y. (2004). Improved monomeric red, orange and yellow fluorescent proteins derived from Discosoma sp. red fluorescent protein. *Nature Biotechnol.* **22**, 1567-1572.

Yang, B., Treweek, J. B., Kulkarni, R. P., Deverman, B. E., Chen, C. K., Lubeck, E., Shah, S., Cai, L., and Gradinaru, V. (2014). Single-cell phenotyping within transparent intact tissue through whole-body clearing. *Cell* **158**, 945-958.

Zufferey, R., Donello, J. E., Trono, T. J., and Hope, T. J. (1999). Woodchuck hepatitis virus posttranscriptional regulatory element enhances expression of transgenes delivered by retroviral vectors. *J. Virol.* **73**, 2886-2892.